ACS OMEGA

Open Access

http://pubs.acs.org/journal/acsodf

Article

Fabrication of Cerium Metal−Organic Frameworks Functionalized with Glutamic Acid for Adsorption of Basic Red 46 from Aqueous Solutions: Kinetics, Thermodynamics, and Optimization

Roaa T. Mogharbel, Omaymah Alaysuy, Ibrahim Saleem S Alatawi, Nadiyah M. Alshammari, Sahar Sallam, Abeer M. Almutairi, Ameena Mohsen Al-Bonayan, and Nashwa M. El-Metwaly*

Cite This: *ACS Omega* 2025, 10, 15096−15115

Read Online

ACCESS | Metrics & More | Article Recommendations | Supporting Information

ABSTRACT: This research investigated the efficient removal of cationic Basic red 46 (BR46) dye from aqueous solutions, by means of cerium metal−organic frameworks (Ce-MOF) functionalized with glutamic acid to create NH_2−Ce-MOF. The NH_2−Ce-MOF was easily produced through a postsynthesis functionalization strategy and extensively analyzed through numerous methods with X-ray diffraction (XRD), scanning electron microscopy (SEM), X-ray photoelectron spectroscopy (XPS), energy dispersive X-ray (EDX), and N_2 adsorption/desorption isotherm. The findings revealed that the synthesized adsorbent had a high surface area of 1158.8 m^2/g, a pore size of 1.511 nm, and a pore volume of 0.875 cm^3/g. Upon adsorption of the BR46 dye, the surface area decreased to 872.6 m^2/g, the pore size reduced to 1.18 nm, and the pore volume released to 0.53 cm^3/g. The decreases in surface area, pore size, and volume demonstrate the material's strong ability to adsorb substances, as the dye molecules can fill the tiny pores. They exhibited an increased adsorption capability of 454.8 mg/g. The Langmuir isotherm and pseudo-second-order kinetic models performed the best at simulating adsorption isotherm and kinetic curves, respectively. The exhibition of chemisorption and adsorption energy of 28.4 kJ/mol was supported by various adsorption driving forces, including hydrogen bonding, electrostatic interaction, $\pi-\pi$ conjugation, pore filling, and van der Waals force. After conducting thorough research on the impact of temperature, it was established that the adsorption procedure is both endothermic, indicated by a positive ΔH° of 83.7 kJ/mol.K, and spontaneous, as confirmed by the increase in negativity of ΔG° with rising temperatures. Additionally, the increase in randomness with increasing temperatures is evident in the ΔS° value of 289.32 J/mol. Employed Box−Behnken design (BBD) and response surface methodology (RSM) to enhance the results of the adsorption procedure. The NH_2−Ce-MOF proposal is a practical, affordable solution for eliminating BR46 dye from wastewater streams because the adsorbent was composed of reusable materials and reused over five times with excellent efficiency.

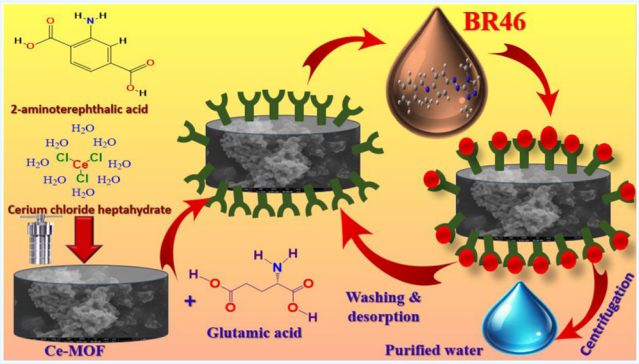

1. INTRODUCTION

To safeguard the environment and public health, industrial colors must be removed from wastewater. These dyes, which are frequently resistant to biodegradation, bring harmful substances into aquatic environments, causing harm to marine organisms and upsetting the natural balance by diminishing sunlight, lowering dissolved oxygen levels, and hindering the photosynthesis process in water-based plants.[1] Moreover, numerous dyes are known to cause cancer, creating significant health hazards if they enter drinking water sources.[2] Wastewater containing dyes that has not been treated can result in a violation of environmental laws, leading to penalties and tighter regulations for industrial facilities.[3] In addition, eliminating dyes creates the opportunity for reusing water, which conserves fresh water supplies and promotes sustainable business practices.[4] Dye pollution also detracts from the natural beauty of bodies of water, negatively impacting tourism and the overall aesthetics of communities. Implementing effective methods to remove dyes, such as adsorption, biodegradation, and advanced oxidation processes, helps to reduce these risks and ensures that industrial procedures adhere to environmental and health guidelines.[5]

The textile industry's industrial processes lead to a substantial release of dyes into wastewater. It is assessed that 10−15% of textile dyes used are missing during manufacturing and end up in wastewater, resulting in approximately 280,000

Received: November 24, 2024
Revised: April 2, 2025
Accepted: April 4, 2025
Published: April 8, 2025

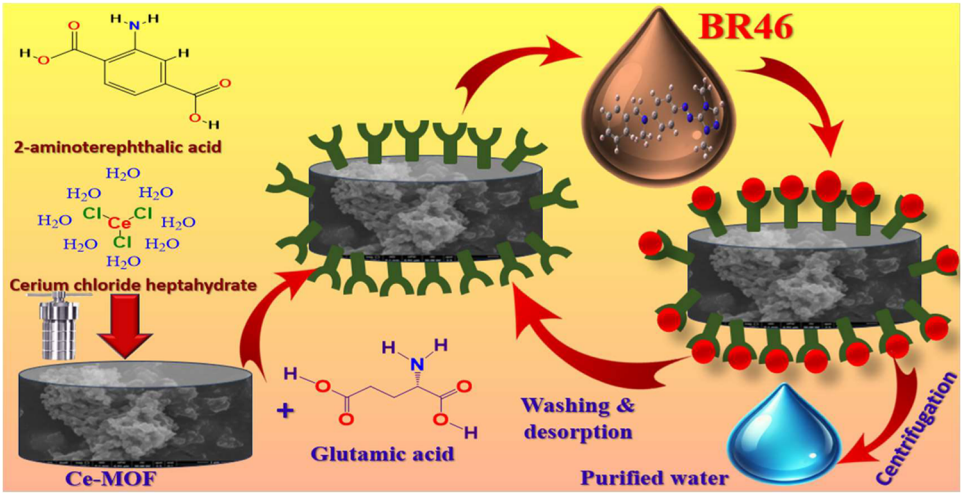

Figure 1. Schematic drawing of the synthesis of NH_2−Ce-MOF and adsorption of the BR46 dye.

tons of textile dyes being released annually into industrial effluents globally.[6] This makes the textile industry the main contributor, responsible for about 54% of dye effluents polluting the environment.[7] These discharges present environmental challenges such as aquatic toxicity and potential human health hazards, highlighting the necessity for effective wastewater treatment and dye recovery methods.[8]

The method of adsorption for eliminating industrial dyes from wastewater has numerous benefits, which contribute to its widespread use in treatment procedures.[9] Its ability to effectively capture a range of dyes, both organic and inorganic, even at low levels, ensures successful dye removal. An important advantage is the cost-efficiency of this method, which frequently makes use of inexpensive materials such as activated carbon, biochar, and agricultural waste products, thus rendering it suitable for widespread use. Adsorption systems are easy to use and upkeep, often needing only basic equipment, thus simplifying operations and cutting down on training needs. This approach is environmentally conscious, utilizing sustainable and biodegradable adsorbents to aid in responsible waste management. In contrast to chemical treatments that could generate hazardous residues or additional pollutants, adsorption typically yields harmless byproducts, thus reducing its environmental footprint. Its capability to be used in a wide series of capacities, from small laboratories to large factories, provides versatility. Moreover, numerous adsorbents can be reused by being heated or washed with chemicals, making the process environmentally friendly and cost-effective in the future.[10] When considered together, these benefits make adsorption a practical, affordable, and environmentally conscious method for removing dyes in industrial settings.[11]

Metal−organic frameworks (MOFs), due to their distinctive structural characteristics and chemical functionalities, present themselves as highly favorable options for the adsorption of dyes.[12] In contrast to conventional substrates, such as silica and carbon, metal−organic frameworks (MOFs) present a distinctive amalgamation of elevated surface area, adjustable porosity, and tailor-made chemical properties. This unique composition facilitates accurate interactions with dye molecules via $\pi-\pi$ stacking, electrostatic interactions, and hydrogen bonding. The materials in question exhibit exceptional selectivity, enabling the precise elimination of particular dyes. Furthermore, they maintain outstanding stability over a broad spectrum of pH levels, overcoming the drawbacks associated with silica, which is prone to dissolution under extreme pH conditions, and with carbon, which suffers from a lack of functional tenability. Furthermore, the existence of unsaturated metal sites within metal−organic frameworks (MOFs) significantly improves their adsorption capability via coordination or ionic interactions, a characteristic that is lacking in both silica and carbon materials. Metal−organic frameworks (MOFs) demonstrate superior performance compared to traditional materials in terms of their regeneration and reusability features.[13] They effectively preserve their structural integrity even after multiple operational cycles. Despite existing challenges associated with cost-effective synthesis and long-term stability, metal−organic frameworks (MOFs) exhibit remarkable adsorption efficiency, selectivity, and versatility. These attributes position MOFs as promising advanced materials specifically suited for the removal of dyes in wastewater treatment processes.[14,15]

Using response surface methodology (RSM) to optimize industrial dye elimination through adsorption processes has several benefits.[16,17] This is due to RSM's ability to simultaneously modify a wide range of limits, such as temperature, contact duration, pH, and adsorbent dosage, to identify the ideal conditions for attaining the maximum degree of dye removal. This approach saves time and money by reducing the need for several tests. Furthermore, it enables researchers to examine how several variables, such as temperature and adsorbent concentration, interact in a manner not possible with conventional single-variable approaches. This gives a more complete picture of how these elements affect the adsorption efficiency. Furthermore, the predictive power of RSM makes it possible to improve mathematical models that forecast adsorption performance under various circumstances.[18,19] This feature makes it possible to choose the best parameters and simulate various situations without requiring more experimental testing. Response surfaces and contour plots from the approach offer a visual depiction of the relationships between variables and adsorption results, which aids in comprehending the effects of various aspects and utilizing this information to enhance the procedure. RSM is adjustable for a variety of adsorption methods and dye types due to its scalability and adaptability, which makes it

https://doi.org/10.1021/acsomega.4c10666
ACS Omega 2025, 10, 15096−15115

appropriate for both small-scale laboratory use and larger industrial needs. Because of these benefits, RSM is a vital instrument for wastewater treatment that produces highly optimized, economical, and efficient dye adsorption results.[20,21]

The novelty of this study was eliminating Basic Red 46 (BR46) dye by synthesized NH_2−Ce-MOFs, which are cerium-based metal−organic frameworks (Ce-MOFs) functionalized with glutamic acid. Glutamic acid functionalization adds amine groups, which improves the material's selectivity and adsorption ability. In order to comprehend their individual and combined effects, the study looked into a number of elements that affect the adsorption procedure, such as pH, initial dye concentration, adsorbent dose, and temperature. Response Surface Methodology (RSM) is also used to optimize the adsorption performance, which makes it likely to regulate ideal circumstances for the highest dye-removal efficacy. This novel blend of functionalized MOFs and cutting-edge optimization methods shows great promise for enhancing dye adsorption efficiency and provides a viable option for wastewater treatment applications.

2. EXPERIMENTAL SECTION

The Supporting Information (Tables S1 and S2) contains information about the supplies and tools.

2.1. Production of Adsorbent. *2.1.1. Production of Ce-MOF.* The cerium metal−organic framework was produced by combining 1.84 g of 2-aminoterephthalic acid in 25.0 mL of methanol and 0.8 g of cerium chloride hexahydrate in 5 mL of distilled water. The conventional hydrothermal synthesis method was employed to mix the solutions after complete desolvation.[22] Inside a Teflon autoclave wall of 100 mL capacity, the combination was subjected to a gradual increase in temperature to 100 °C over 24 h. Following this, the substance underwent centrifugation and was washed twice with deionized water. Following that, it was dried overnight at 80 °C (Figure 1).[23]

2.1.2. Production of NH_2−Ce-MOF. The combination of Ce-MOF and glutamic acid was evenly mixed in a solution of DMF and ethylene glycol and left to stir at room temperature for 4 h. The resulting mixture was then centrifuged to produce NH_2−Ce-MOF powder, which was subsequently dried overnight at 80 °C.[24] The mixture was subjected to heating for a full day at a steady increase of 5 °C/min, reaching a temperature of 100 °C in a Teflon autoclave with a 100 mL wall. After cooling, the material went through three washes with deionized water before being centrifuged. After that, it was dried at 80 °C for the entire night (Figure 1).

2.2. Removal and Batch Studies of the NH_2−Ce-MOF. The study assessed the efficacy of NH_2−Ce-MOF in removing the BR46 dye from aqueous solutions by analyzing its removal efficiency and absorption capacity. The influence of varying the solution's pH (from 2.0 to 12.0), the quantity of adsorbent used (0.02−0.50 g), and the duration of adsorption (0−100 min) were investigated. A thermostatic Shaker water bath was used for batch adsorption investigations at 25 °C by a predetermined agitation speed of 180 rpm.[17,25] The ultraviolet−visible (UV−vis) spectrophotometer was used to measure the absorbance (at a wavelength of 538 nm) of the dye at numerous concentrations.[12,17] A 250 mL flask enclosing a fixed volume of BR46 dye was employed for the removal studies (25 mL).[26] Analysis was conducted on the kinetic, thermodynamic, and isothermal limits and eq 1 was employed to assess the elimination efficiency and adsorption capability (q_e, mg/g). Furthermore, the adsorption capability was determined by means of eq 2. These calculations were performed in accordance with the specified formulas

$$\%R = \frac{(C_i - C_t)}{C_i} \times 100 \tag{1}$$

$$q_e = \frac{(C_i - C_t)V}{M} \tag{2}$$

where C_i (mg/L) is the original dye concentration, C_t (mg/L) is the concentration of dye at any given time t, M (g) is the mass of the adsorbent, and V (L) is the volume of the solution.

2.3. Experimental Design. Response Surface Methodology (RSM) is a typical mathematical and statistical tool that can be utilized to create, enhance, and streamline processes. The goal is to maximize a positive outcome that is influenced by multiple factors. Typically, a complete quadratic equation is employed in RSM, and the second-order model is represented by the eq 3

$$Y = \beta_o + \sum \beta_i X_i + \sum \beta_{ii} X_i^2 \sum \sum \beta_{ij} + X_i X_j \tag{3}$$

Based on the formula, Y is the anticipated outcome, β_o is the constant coefficient, β_i refers to the linear factors, β_{ii} denotes the squared factors, β_{ij} signifies the interaction factors, and X_i and X_j are used to denote the independent variables. The central composite design (CCD) and response surface methodology (RSM) are well-suited for establishing a quadratic model to improve key variables and analyze the relationship and interaction of parameters with a minimal number of experiments.[27−29] In this current investigation, a central composite design (CCD) incorporating three variables was utilized to demonstrate the association among adsorption capability between dyes and the factors of adsorbent dose (X1), contact time (X2), and pH of Basic Red 46 dye solution (X3).[30] The Design Expert Software has compiled extensive data containing the maximum and minimum values for each factor (Table S3). The table provides a comprehensive display of various parameter combinations and their respective results, including ″2n″ axial designs, P-center designs, and designs with 2n factorial runs.[12] Equation 4 provides a method for determining the quantity of experimentation that is contingent on the quantity of input factors

$$N_p = [2^m + (2 \times m) + P] = [2^3 + (2 \times 3) + 3] = 17 \tag{4}$$

The letter "p" represents the quantity of required experimental tests, while "N" indicates the number of procedural factors impacting the outcomes. The "m" value in the ongoing analysis is 3.[25] The Central Composite design consists of three primary phases: calculating the model constants, setting up the investigational design, and forecasting the model's performance while assessing the results. After completion, a model is created by using actual data to examine how the function functions with various input variable combinations. Table S3 displays the layout of the experiments, detailing the variable values used in the calculated matrix. Analysis of Variances (ANOVA) was used to evaluate the model's validity. This included a discussion of R^2 values, coefficient of difference, and the accuracy of the response surface model, as determined by lack of fit (LOF) analysis.

https://doi.org/10.1021/acsomega.4c10666
ACS Omega 2025, 10, 15096−15115

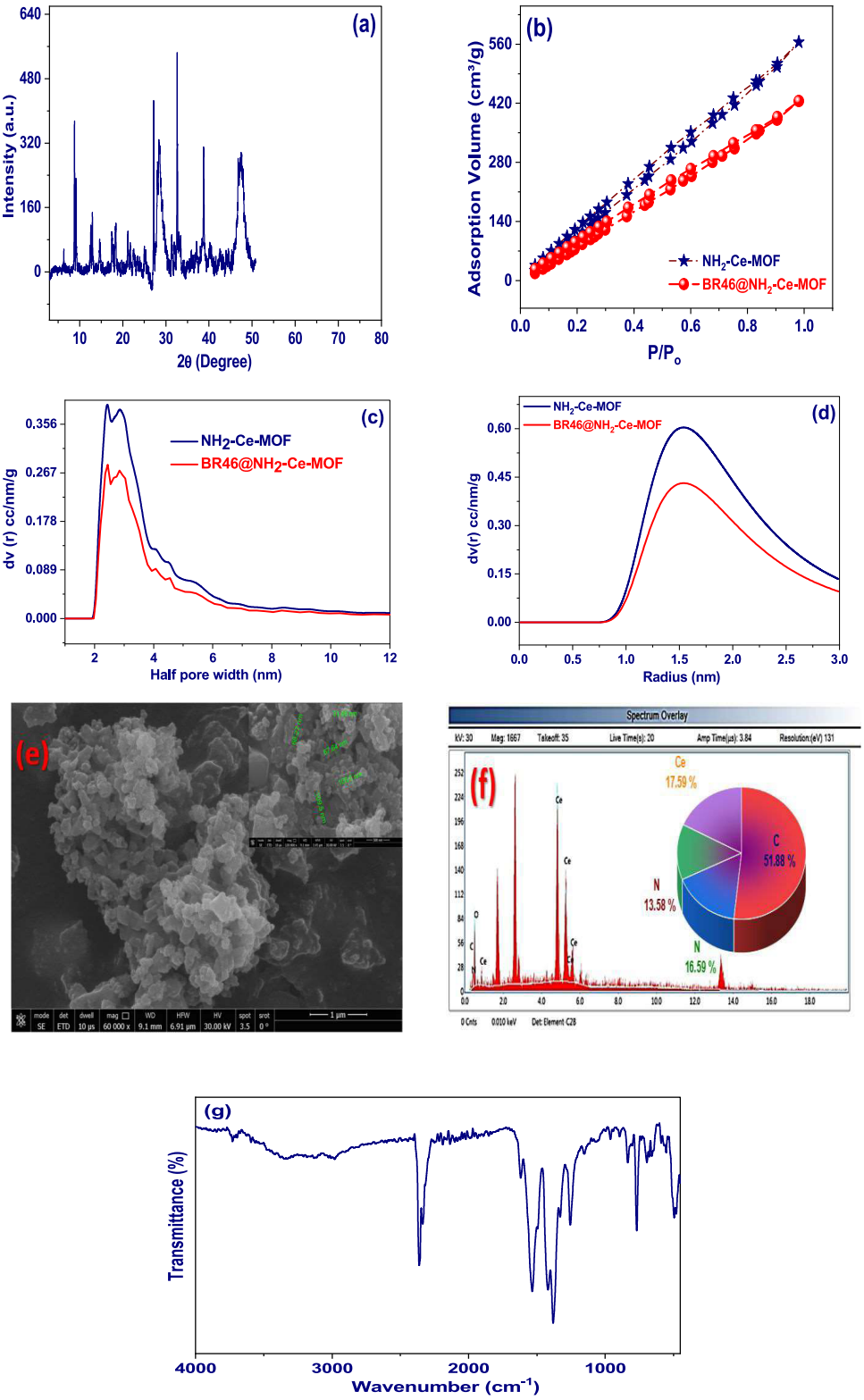

Figure 2. (a) XRD pattern, (b) N_2 adsorption/desorption isotherm, (c) pore size distribution, (d) pore radius distribution, (e) SEM image, (f) EDX image of NH_2−Ce-MOF, and (g) FTIR spectrum of NH_2−Ce-MOF.

3. RESULTS AND DISCUSSION

3.1. Description of NH_2−Ce-MOF. *3.1.1. X-ray Diffraction Patterns (XRD).* The analysis in Figure 2(a) shows that the NH_2−Ce-MOF exhibits a high degree of crystallinity. By means of the Foolproof and Check Cell tools, it was determined that the adsorbent organization possesses an orthorhombic crystal assembly in the P222 space group, as detailed in Table S4. The crystal dimensions were gained from the designed limits: a = 8.93 Å, b = 11.52 Å, c = 6.83 Å, α = 90°, β = 90.12°, γ = 90°.[30−32] The diffraction peaks of NH_2−Ce-MOF remained intact even after adsorption, as gotten in

https://doi.org/10.1021/acsomega.4c10666
ACS Omega 2025, 10, 15096−15115

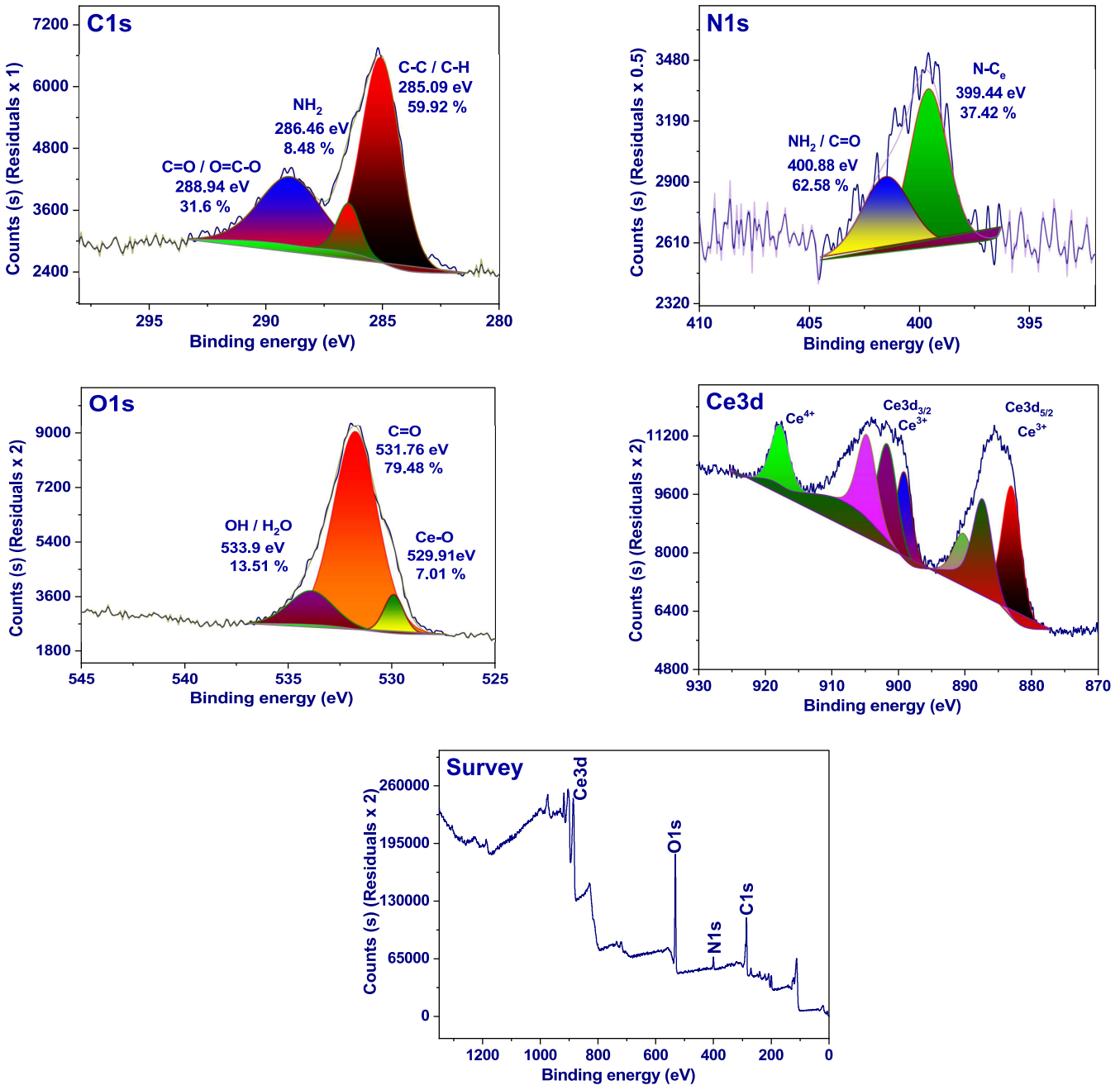

Figure 3. XPS of NH_2−Ce-MOF.

Figure 2(a), indicating the exceptional stability of the crystal structure.[32,33]

3.1.2. N_2 Adsorption/Desorption Isotherm. The N_2 adsorption/desorption isotherm exhibited by NH_2−Ce-MOF, which has an initial surface area of 1158.8 m^2/g, a pore size of 1.511 nm, and a pore volume of 0.875 cm^3/g, demonstrates features of a Type I isotherm commonly seen in microporous materials. The profile of this isotherm indicates quick adsorption at low relative pressures (P/P_o), and then leveling off as the pores become saturated, demonstrating considerable microporosity. After the dye BR46 is adsorbed, the surface area experiences a decrease to 872.6 m^2/g, the pore size is reduced to 1.18 nm, and the pore volume decreases to 0.53 cm^3/g. The decreases in surface area, pore size, and volume emphasize the substance's ability to adsorb effectively, as the dye molecules are able to fill the microspores.[34] This suggests that NH_2−Ce-MOF could be used for removing dyes or contaminants (Figure 2(b)).

The ($dv(r)$) graph, with the x-axis representing half of the pore width, depicts the distribution of pore sizes in NH_2−Ce-MOF both before and after the absorption of BR46 dye. Initially, NH_2−Ce-MOF displays a noticeable peak at a half-pore width of roughly 2 nm, suggesting the existence of micropores. The peak's intensity decreases after BR46 adsorption (red curve), indicating that the dye molecules take up some of the pore space, thereby reducing the overall accessible pore volume in this range. The reduction in the peak's strength following adsorption suggests that BR46 dye is filling up smaller pores, resulting in a decrease in the overall micropore volume. This adsorption pattern emphasizes the

https://doi.org/10.1021/acsomega.4c10666
ACS Omega 2025, 10, 15096−15115

material's capacity to trap dye molecules, especially within its microporous framework, which could prove advantageous for use in contaminant elimination or environmental restoration.[35] The small decline in a variety of larger pore diameters also indicates that only partial adsorption occurs in the mesopores. This enhances the versatility of the material as an adsorbent for molecules of different sizes, as shown in Figure 2(c).

Figure 2(d) displays the ($dv(r)$) graph for NH_2−Ce-MOF, revealing a prominent peak at approximately 1.5 nm. This peak confirms the presence of a high concentration of micropores near this radius. Upon adsorption of the BR46 dye, indicated by the red curve, there is a noticeable decrease in the intensity of the peak as well as a slight shift toward smaller radii. This suggests that the dye molecules fill the pores and decrease their accessibility. The decrease in ($dv(r)$) values indicates a reduction in both pore volume and surface area, which aligns with the initial examination of the material's ability to adsorb dye. The disparity between the two curves emphasizes how extensively BR46 dye molecules infiltrate and fill the micropores. This supports the conclusion that NH_2−Ce-MOF possesses formidable adsorption abilities for this dye, rendering it viable for use in environmental cleanup or related areas concerned with removing contaminants from solutions.[36]

3.1.3. SEM Analysis. The scanning electron microscopy (SEM) image reveals the NH_2−Ce-MOF as having a porous and irregular shape, with particles ranging in size from around 31.48 to 109.5 nm. The presence of visible structures and particle clusters suggests a rough surface, potentially enhancing its adsorption capabilities through an enlarged surface area.[37] The size of these particles, particularly the existence of tiny details, corresponds to the material's microporous and possibly mesoporous characteristics as seen in the adsorption isotherms besides pore size distribution information. The observed variation in particle sizes, ranging from 31 to over 100 nm, indicates a hierarchical structure that could potentially improve adsorption effectiveness. The variety of particle sizes and the rough texture observed are encouraging characteristics for use in adsorption, as they are likely to offer numerous attachment sites for dyes or contaminants (Figure 2(e)).

3.1.4. EDX Analysis. The energy dispersive X-ray (EDX) spectrum attached presents a thorough examination of the elemental makeup of NH_2−Ce-MOF, confirming the presence and quantities of important elements such as carbon (C), nitrogen (N), oxygen (O), and cerium (Ce). Carbon makes up the majority of the composition at 51.88%, indicating its likely role as the primary component of the organic linkers in the MOF structure. Nitrogen, comprising 16.59%, aligns with NH_2-functionalization, suggesting the existence of amino groups that enhance the functionality of the framework. In smaller quantities, oxygen may play a role as part of the organic ligands or cerium complexes.[38] The 17.59% cerium content is essential to the framework, acting as the metal node that connects the organic ligands and ensures structural stability. The atomic percentages are further depicted in the pie chart, providing a visual representation of the high concentration of carbon as well as the attendance of cerium, nitrogen, and oxygen. The elemental composition of NH_2−Ce-MOF is confirmed by the EDX spectrum, indicating that it could be useful for adsorption or catalysis because of the combined presence of cerium and functional NH_2 groups in the framework (Figure 2(f)).

3.1.5. FTIR. The distinctive bands in the NH_2−Ce-MOF Fourier Transform Infrared (FTIR) spectrum are associated with the organic ligand (Figure 2(g)). The overlapping υ(OH) and υ(NH) vibrations are responsible for the broad absorption band, which reaches its maximum at 3345 cm^{-1}. On the other hand, the C−H group's stretching asymmetric and symmetrical vibrations were attributed to the two distinct bands located at 3131 and 2971 cm^{-1}, respectively. Two bands at 1616 and 1376 cm^{-1} that correspond to the symmetric and asymmetric stretching modes, respectively, define the carboxylic group. The band at 1540 cm^{-1} represents the carboxylic groups' C═O stretching vibrations. This peak at 1424 cm^{-1} is ascribed to the C═C group's stretching vibration. The band at 1260 cm^{-1} was associated with the ligand's aromatic −CH. The peak seen at 495 cm^{-1} confirmed the presence of Ce−O.

3.1.6. XPS. The XPS survey spectrum of the NH_2−Ce-MOF offers a thorough depiction of the material's elemental composition through the display of peaks associated with different binding energies. The marked high points are indicated as Ce 3d, O 1s, N 1s, and C 1s, which correspond to the key components found in the arrangement, cerium (Ce), oxygen (O), nitrogen (N), and carbon (C).

The X-ray Photoelectron Spectroscopy (XPS) analysis of the C 1s peak in the NH_2−Ce-MOF reveals specific peaks indicating different carbon bonding settings and oxidation states present in the material. The dominant peak at 285.09 eV is linked to C−C or C−H bonds, which are indicative of aliphatic carbon within the structure. The peak at 286.46 eV is indicative of C−O or C−N bonds, potentially stemming from amino ($-NH_2$) or hydroxyl (−OH) groups connected to the MOF. Meanwhile, the peak near 288.94 eV points to carbonyl (C═O) or carboxylate (O═C−O) functionalities, likely originating from bonding within the MOF framework or minor oxidation[21] (Figure 3).

The XPS data display two clear peaks in the N 1s area of the NH_2−Ce-MOF spectrum, which indicate the presence of diverse nitrogen bonding settings within the material. The main peak, which appears at 400.8 eV, is commonly linked to nitrogen present in amine ($-NH_2$) or imine (C═N) groups, signifying the presence of amino functionalization on the MOF structure.[16,39] The secondary peak, with slightly lower binding energy, could indicate nitrogen atoms involved in more intricate bonding, such as metal−nitrogen interactions (N−Ce) or potentially minor deviations resulting from structural or environmental factors within the MOF. The colored areas under the peaks illustrate the presence of fitted components, offering valuable information about the nitrogen's nature and integration in the material. This confirms the existence of amino functionalities and suggests possible coordination interactions with cerium in the MOF.[39]

The analysis of the XPS spectrum for the O 1s region of the NH_2−Ce-MOF demonstrates the presence of three prominent peaks, with each peak corresponding to a unique oxygen bonding state within the structure. This indicates the existence of distinct oxygen bonding states within the NH_2−Ce-MOF, as revealed by XPS analysis. The primary peak at 529.91 eV is usually linked to metal−oxygen (M−O) connections, which in this scenario are probably related to cerium−oxygen interactions (Ce−O) within the MOF structure.[40,41] The appearance of a second peak at approximately 531.76 eV could be linked to the presence of oxygen in hydroxyl (O−H) groups or potentially in C═O bonds. This suggests the existence of functional groups that affect the chemical makeup of the framework. The presence of a smaller peak at approximately 533.9 eV is commonly indicative of the presence of oxygen

https://doi.org/10.1021/acsomega.4c10666
ACS Omega 2025, 10, 15096−15115

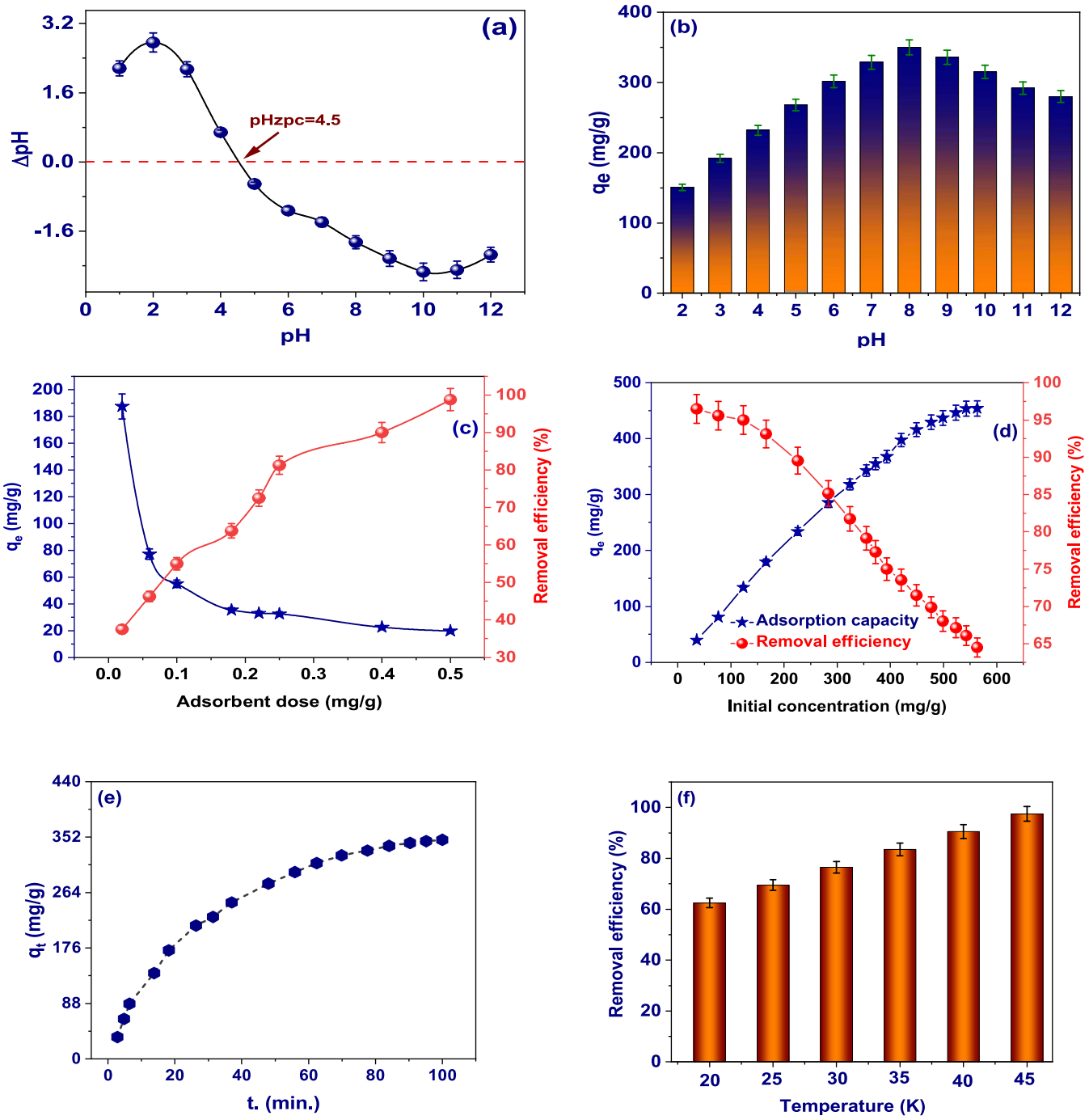

Figure 4. (a) Determination of pH_{zpc}, (b) effect of pH (pH: 2 to 12, C_i: 400 mg/L, dose: 0.02 g, T: 25 °C, and time: 30 min.), (c) effect of the adsorbent dose (pH: 8, C_i: 400 mg/L, dose: 0.02 to 0.25 g, T: 25 °C, and time: 30 min.), (d) original concentration effect (pH: 8, C_i: 35 to 560 mg/L, dose: 0.02 g, T: 25 °C, and time: 100 min.), (e) time effect (pH: 8, C_i: 400 mg/L, dose: 0.02 g, T: 25 °C, and time: 5 to 100 min.), and (f) temperature effect (pH: 8, C_i: 400 mg/L, dose: 0.02 g, T: 20 to 45 °C, and time: 5 to 100 min.).

atoms in adsorbed water or weakly bonded hydroxyls. These may result from environmental exposure or minimal hydration of the material. The colored areas on the various fitted components offer valuable information about the bonding structure and composition of oxygen species within the NH_2−Ce-MOF (Figure 3).

The XPS examination of the Ce 3d region in NH_2−Ce-MOF reveals several distinct peaks, providing insights into the oxidation states and electronic landscape of cerium in the material. The intricate arrangement of peaks in the spectrum, spanning a wide range of binding energies (around 880−930 eV), indicates the existence of both Ce^{3+} and Ce^{4+} states. The peaks with higher energy values (around 916−920 eV) are commonly connected to the Ce^{4+} $3d^{3/2}$ and $3d^{5/2}$ states, which signify the presence of oxidized cerium. On the other hand, the peaks with lower energy levels (approximately 880−890 eV) are associated with Ce^{3+}, indicating the presence of reduced cerium in the structure. A mixed-valence state, which is typical of cerium-based MOFs and is advantageous for catalytic and electronic applications, is implied by the combination of these

https://doi.org/10.1021/acsomega.4c10666
ACS Omega 2025, 10, 15096−15115

states. The shaded sections beneath the individual peaks demonstrate the components that have been fitted, helping to differentiate the precise distribution of Ce^{3+} and Ce^{4+}, which is crucial for comprehending the redox characteristics and durability of the NH_2−Ce-MOF.[28]

3.2. Batch Experiments. *3.2.1. Effect of pH and Point of Zero Charge.* The pH of the solution has a major effect on an adsorbent's ability to remove contaminants. This is because it affects the adsorbent's functional groups' surface charge characteristics, ionization state, and degree of dissociation. By taking into account the pH values at the adsorbents' zero charge sites (pH_{PZC}), the behavior can be explained. The pH value of 4.5 was determined for NH_2−Ce-MOF in Figure 4(a). When the pH of the solution is lesser than the pH_{PZC} (pH < 4.5), the hydrogel beads of NH_2−Ce-MOF become positively charged (due to excess H^+), which results in strong repulsion with dye molecules of similar charge, ultimately reducing the efficiency of adsorption. For pH values higher than the pH_{PZC} (pH greater than 4.5), the beads' surface is mainly covered with negative charges. This makes it easier for cationic dyes (such as BR46) to be attracted to the beads, resulting in the most effective absorption of this dye within those pH ranges. The impact of the pH level of solutions on how effectively the dye BR46 dye is removed was observed within a pH series of 2 to 12, as depicted in Figure 4(b). Conversely, with the rise in solution pH, the NH_2−Ce-MOF adsorbent surface saw a gradual deprotonation of functional groups (hydroxyl and carboxylate), resulting in an increased retention of dye molecules.[42]

3.2.2. Effect of Dose. Batch studies were carried out using 25 mL of BR46 dye solutions at 400 mg/L, adding varying quantities of adsorbent from 0.20 to 0.25 g in order to assess the ideal quantity of crude clay to add to an aqueous dye solution (Figure 4(c)). It was discovered that while the adsorption capability failed with increasing adsorbent dose, the removal efficiency rose. This suggests that an increased mass of the adsorbent led to a greater amount of adsorption sites. This can be because there are extra adsorption sites and the adsorbent has a higher surface area.[43]

3.2.3. Effect of the BR46 Dye Concentration. Figure 4(d) depicts how the original dye concentration affects the rate at which the BR46 dye is adsorbed at pH 8 and 293 K. When the original dye concentration increases, so does the adsorption capacity. The adsorption capacity of dye on NH_2−Ce-MOF fluctuates from 39.6 to 454 mg/g as the original dye concentration increases from 35 to 560 mg/L. This implies that the original dye concentration has a main influence on the dye's adsorption capability. Furthermore, when the mass transfer driving force increased, the barrier to dye uptake reduced, resulting in a higher initial rate of adsorption for higher initial dye concentrations.[44]

3.2.4. Effect of Contact Time and Temperature. The influence of temperature on the effectiveness of NH_2−Ce-MOF in removing BR46 dye was designed within the range of 20 to 45 °C, and the findings are represented in Figure 4(e,f) in relation to contact time. Both figures clearly show that as the temperature rises the dye-removal process also rises. This indicates that the adsorption technique is endothermic and that higher temperatures have a positive impact on the formation of radical species and their interactions.[45]

3.3. Adsorption Isotherm. Utilizing adsorption isotherm models such as Langmuir,[46] Freundlich,[47] Dubinin−Radushkevich (D−R),[47] and Temkin greatly aids in studying BR46 dye adsorption onto NH_2−Ce-MOF, as each model presents a unique view of the adsorption behavior.[48] The Langmuir isotherm assumes monolayer adsorption on a homogeneous surface, helping to determine the maximum adsorption capacity (q_{max}) of NH_2−Ce-MOF essential for managing dye loads and industrial scaling. The Freundlich isotherm, suited for nonuniform surfaces, provides insights into adsorption intensity ($1/n$) and illustrates how surface variability influences the process, shedding light on NH_2−Ce-MOF's capacity for BR46 dye at various concentrations.[49,50] The D−R isotherm assesses the average adsorption energy (E), distinguishing between chemical and physical adsorption mechanisms, which aids in determining whether the interaction with BR46 is weak physisorption or stronger chemisorption, informing optimization. The Temkin isotherm evaluates heat changes during adsorption, helping to identify if the process absorbs or releases heat, crucial for determining the optimal dye-removal temperature. Together, these models yield extensive insights into adsorption capacity, interaction intensity, energy characteristics, and thermodynamics, enabling precise management of the operational conditions. This combined approach enhances NH_2−Ce-MOF's efficiency for BR46 dye removal, improving the predictability and effectiveness of wastewater treatment processes.[51]

The Langmuir adsorption isotherm model explains the interaction between BR46 dye molecules and NH_2−Ce-MOF, positing monolayer adsorption on a uniform surface with identical sites as shown in Table S5. Key model parameters reveal insights into the adsorption process's effectiveness.[46] The Langmuir constant (K_L) is 0.017 L/mg, reflecting a moderate attraction between NH_2−Ce-MOF and BR46, suggesting an effective interaction. The maximum adsorption capability of 454.8 mg/g indicates a strong dye-removal capacity, establishing NH_2−Ce-MOF as efficient for adsorption applications. Additionally, the dimensionless separation factor at 0.56 supports the favorable nature of the adsorption, as (R_L) ranges from 0 to 1, confirming NH_2−Ce-MOF's capacity to adsorb BR46 effectively. These findings highlight NH_2−Ce-MOF as an ideal adsorbent for BR46 dye removal in wastewater treatment (Table S6).

The Freundlich adsorption isotherm model provides crucial insights into the adsorption behavior of BR46 dye on NH_2−Ce-MOF. It highlights how the heterogeneous surface of NH_2−Ce-MOF, with its varied adsorption sites, interacts with the dye. The Freundlich constant (K_F) of 49.61 (mg/g) (L/mg)$^{1/n}$ signifies that NH_2−Ce-MOF exhibits a high adsorption capability, particularly at low dye concentrations, showcasing its effectiveness in capturing the dye. A high K_F value suggests strong attraction to BR46 dye, enabling significant absorption of dye molecules in low-concentration solutions. The intensity parameter (n = 2.33) supports the favorable adsorption process, with a value of over 1 indicating enhanced efficiency at lower dye concentrations and reduced intensity at higher levels. This suggests NH_2−Ce-MOF efficiently captures BR46 dye, particularly when concentrations fluctuate, as it effectively attracts and binds the dye at low levels.[15] The Freundlich model emphasizes surface heterogeneity, indicating that NH_2−Ce-MOF has multiple active sites with different affinities, enabling effective management of the BR46 dye at various concentrations. Thus, NH_2−Ce-MOF is a versatile and effective adsorbent, reliably removing BR46 dye from wastewater, even with changing concentrations. It proves suitable for

https://doi.org/10.1021/acsomega.4c10666
ACS Omega 2025, 10, 15096−15115

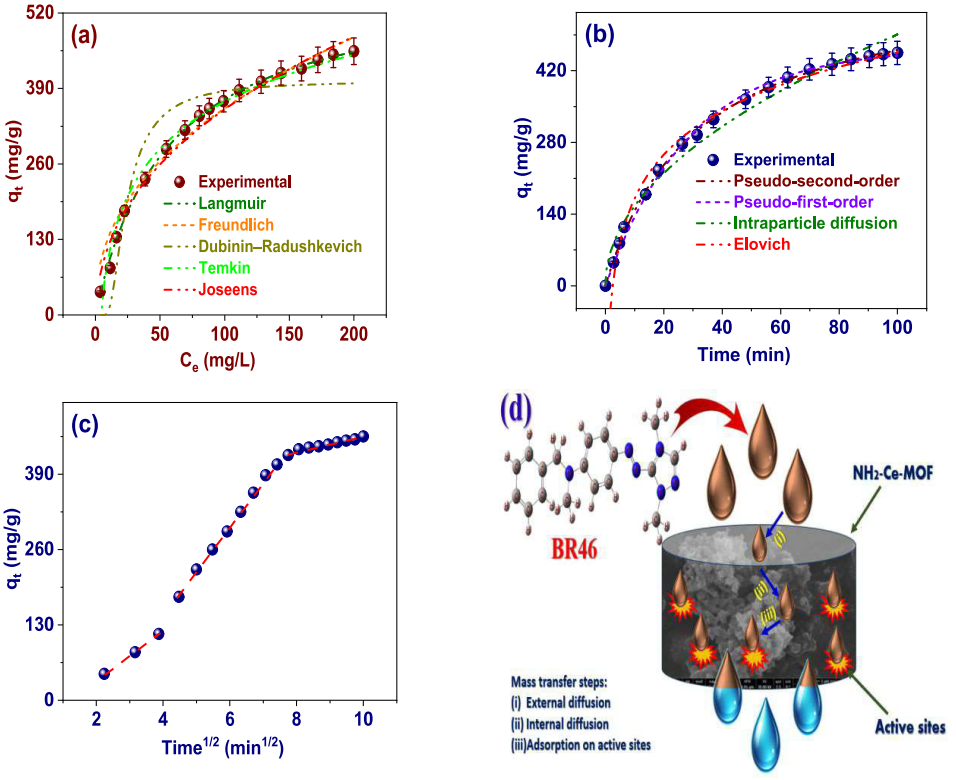

Figure 5. (a) Adsorption isotherm models, (b) adsorption kinetic models, (c) IPD mechanism, and (d) schematic illustration of the diffusion mechanism.

practical wastewater treatment applications, as illustrated in Figure 5(a).[47]

The Dubinin−Radushkevich (D−R) model examines the adsorption of BR46 dye onto NH_2−Ce-MOF, focusing on adsorption capacity, interaction energy, and mechanism.[52] NH_2−Ce-MOF shows a high D−R saturation capacity (Q_{DR}) of 403.16 mg/g, indicating its effectiveness for wastewater treatment with high dye concentrations. The D−R constant (K_{DR} = 7.4 × 10^{-5} mol^2 kJ^{-2}) reflects a moderate interaction energy, suggesting a balance between stability and strength in the adsorption, allowing for possible desorption if necessary. The average adsorption energy (E_a) of 28.4 kJ/mol implies chemisorptive characteristics since values over 16.0 kJ/mol indicate chemical, rather than physical, adsorption. In conclusion, the D−R model confirms that NH_2−Ce-MOF is a reliable adsorbent for BR46 removal due to its high capacity and stable chemisorptive binding, making it suitable for effective wastewater dye removal.[53]

The Temkin adsorption isotherm model analyzes the adsorption of BR46 dye on NH_2−Ce-MOF, focusing on the interactions between the dye and adsorbent affecting adsorption energy as surface coverage varies.[48] The Temkin constant b_T of 15.84 J/mol indicates a moderate heat of adsorption, reflecting balanced interactions without an excessive energy release. Consequently, the adsorption proceeds steadily as the dye covers the surface. The K_T value of 0.23 L/mol shows NH_2−Ce-MOF's decent affinity for BR46 dye, facilitating effective capture, particularly at lower concentrations. This equilibrium constant suggests moderate efficiency, and these parameters indicate a stable adsorption process with controllable energy and reliable binding strength, enabling effective dye removal. NH_2−Ce-MOF remains efficient even at higher surface saturation, making it a consistent and stable material for wastewater treatment with BR46 dye across various concentrations.[54]

The Jossens adsorption isotherm model enhances our understanding of BR46 dye adsorption onto NH_2−Ce-MOF, focusing on the capacity, affinity, and interaction strength. With a high adsorption affinity constant of 57.83, NH_2−Ce-MOF shows a strong attraction and significant capacity for capturing BR46 dye, even at varying concentrations. The moderate bonding strength indicated by the adsorption intensity constant (J = 0.05) suggests effective retention of BR46 dye molecules while allowing potential release for restoration.[37,55] This balance between strong affinity and moderate interaction intensity makes NH_2−Ce-MOF an effective, reusable adsorbent for sustainable wastewater treatment.[56]

3.4. Adsorption Kinetics. Applying models of adsorption kinetics such as pseudo-first-order,[57] pseudo-second-order,[58] intraparticle diffusion,[59] and Elovich offers insights into BR46 dye elimination via NH_2−Ce-MOF.[60] These models elucidate mechanisms, with pseudo-first-order linked to physisorption and pseudo-second-order indicating chemisorption, allowing accurate predictions of adsorption rates and contact durations. The Intraparticle Diffusion model highlights the effect of diffusion limitations, while the Elovich model reveals the reactivity of diverse surface sites. This analysis aids in optimizing the structure and conditions of NH_2−Ce-MOF, enhancing the efficiency.

Utilizing the pseudo-first-order adsorption kinetic model to study BR46 dye elimination with NH_2−Ce-MOF shows clear advantages. It provides a straightforward means to evaluate the adsorption rate, especially when physisorption predominates.[57]

https://doi.org/10.1021/acsomega.4c10666
ACS Omega 2025, 10, 15096−15115

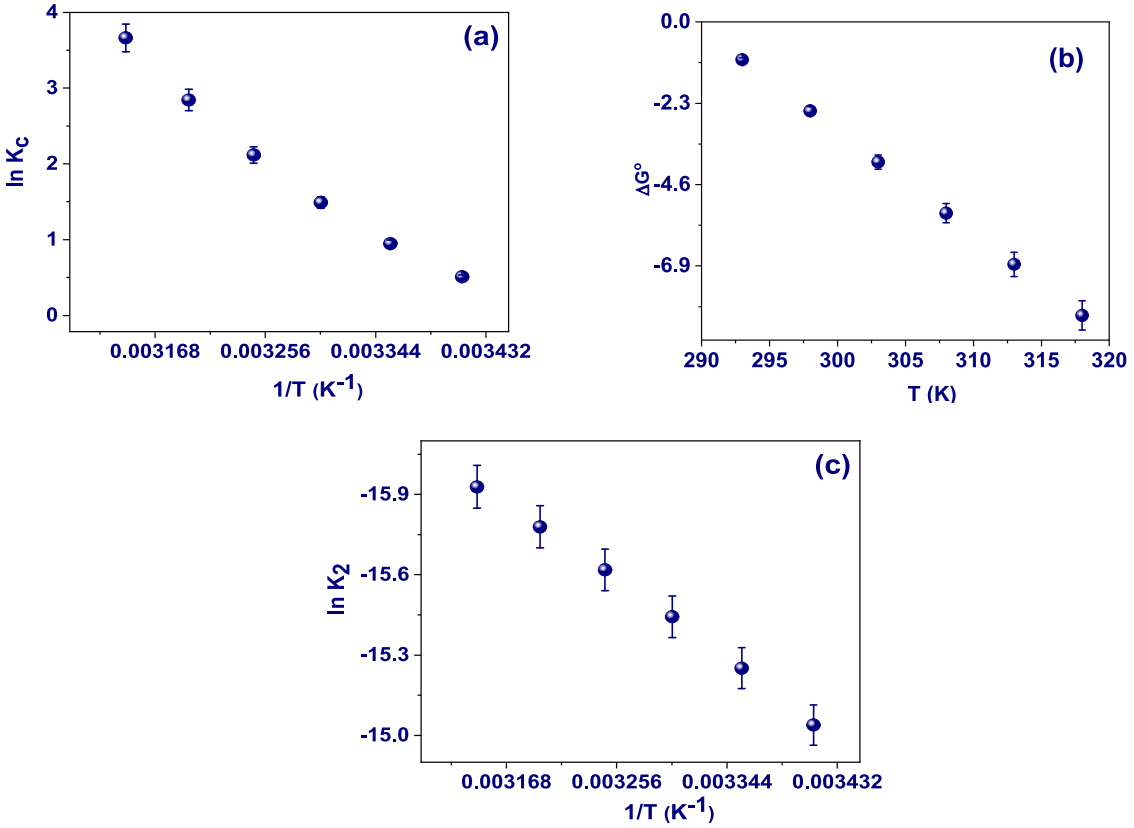

Figure 6. (a) Van't Hoff thermodynamic adsorption model, (b) Effect of temperature on Free Gibb's energy, and (c) Arrhenius model.

This model helps predict the rate at which BR46 is absorbed onto NH_2−Ce-MOF, assisting in optimizing contact times and dosing for effective dye removal. The low-rate constant (K_1 = 0.034 $min^{-1} \times 10^{-2}$) suggests a gradual adsorption process. Optimizing factors such as the adsorbent's surface area and environmental conditions (pH and temperature) can enhance adsorption efficiency. Overall, this model aids in understanding adsorption kinetics and improving NH_2−Ce-MOF's practical application in dye removal (Table S5).

Utilizing the pseudo-second-order model, particularly the adsorption kinetic model, yields valuable insights into the elimination of BR46 dye by NH_2−Ce-MOF. The model's results, including a rate constant of $K_2 = 5.32 \times 10^{-5}$ (g mg^{-1} min^{-1}) $\times 10^{-2}$ and an equilibrium adsorption ability of q_e = 457.8 mg/g, suggest that the adsorption procedure may be primarily subjective by chemisorption. This includes electron distribution or conversation among BR46 and the active sites of NH_2−Ce-MOF. The substantial (q_e) value indicates that NH_2−Ce-MOF is highly effective in adsorbing BR46 due to its significant adsorption capacity, as shown in Figure 5(b). Additionally, the pseudo-second-order model offers precise consideration of the rate and capability of adsorption, enabling exact fine-tuning of the process variables like the amount of adsorbent and duration of contact to attain optimal efficiency.[58] This particular model is valuable for creating and expanding the process in real-world situations. It helps to guarantee consistent and effective adsorption performance under different conditions, which is crucial for water treatment systems (Table S7).

Employing the adsorption kinetic model, specifically the Intraparticle Diffusion model, delivers significant benefits in studying the adsorption and elimination of BR46 dye through NH_2−Ce-MOF. This is especially evident with an intraparticle diffusion rate constant (K_i = 49.05 mg g^{-1} $min^{1/2}$) and intercept (X = 26.22 mg/g).[49] This model is used to determine whether the rate of adsorption is governed by the diffusion process within the pores of the NH_2−Ce-MOF material. The parameter (K_i) represents the speed at which the BR46 dye moves into the pores, and the intercept (X) indicates the presence of a boundary layer effect that may impact the adsorption process. Through the examination of these figures, scientists are able to fine-tune the physical characteristics of NH_2−Ce-MOF, including pore size and surface area, in order to increase the rate of diffusion and enhance the effectiveness of dye removal.[59]

Utilizing the Elovich model within adsorption kinetics to examine the adsorption and elimination of BR46 dye by NH_2−Ce-MOF offers significant insights. The Elovich parameters (β at 123.6 g/mg) and (α at 0.03 mg g^{-1} min^{-1}) are crucial in this analysis. The Elovich model is advantageous for heterogeneous adsorption systems, as it accounts for variations in adsorption energies across different surface sites. The high (β) indicates a reduction in adsorption rate with increased surface coverage, while the low (α) suggests a slower initial adsorption rate. This model assesses the activity of the NH_2−Ce-MOF surface and identifies various active sites with different affinities for BR46 dye. It provides a precise portrayal of adsorption on diverse surfaces and helps fine-tune parameters such as temperature and dye concentration for optimal efficiency. Understanding this is essential for developing NH_2−Ce-MOF materials that effectively capture BR46 dye, ensuring scalable dye removal in water treatment processes.[60]

3.5. Diffusion Mechanism. The phase that controls the rate and mechanism of diffusion during adsorption is better

https://doi.org/10.1021/acsomega.4c10666
ACS Omega 2025, 10, 15096−15115

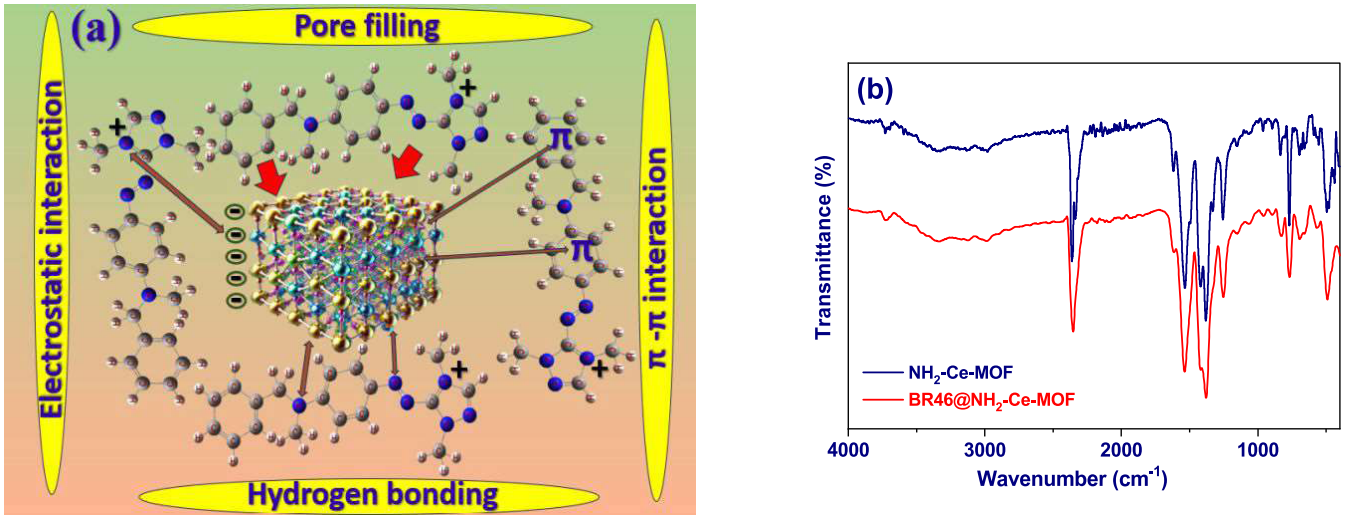

Figure 7. (a) Diagrammatic representation of the mechanism of interaction between BR46 dye and NH_2−Ce-MOF, and (b) FTIR spectra of NH_2−Ce-MOF and BR46@NH_2−Ce-MOF.

understood thanks to the diffusion models.[55] The four distinct phases of adsorption kinetics are (i) Mass transfer is how the adsorbate moves from the bulk solution to the adsorbent's exterior; (ii) The way molecules propagate across the layer at the border; (iii) The movement of adsorbate molecules from the adsorbent material's outer surface to its interior pores; and (iv) Coverage of the binding places of the adsorbent can be observed in Figure 5(c,d).

3.6. Thermodynamics. One important aspect affecting a substance's capacity to absorb dyes is temperature. The absorption of BR46 dye by NH_2−Ce-MOF was calculated at three dissimilar temperatures, 298, 308, and 318 K. Table S5 exhibits the thermodynamic values, such as standard enthalpy $\Delta H°$, standard entropy $\Delta S°$, and Gibbs free energy $\Delta G°$, determined by means of eqs S9 and S10 (Table S5).[61] The absorption of BR46 dye onto NH_2−Ce-MOF is shown to be endothermic based on the positive $\Delta H°$ value in Table S8 and Figure 6(a,b).[30,34] The adsorbent surface and BR46 dye interface exhibit greater disorder, as suggested by the positive $\Delta S°$ values. With rising temperature, the $\Delta G°$ value declines, resulting in an increase in the reaction's spontaneity.[62] This implies that increased temperatures contribute to the progression of the reaction shown in Figure 6(c). It can be inferred that the bonding of BR46 dye to NH_2−Ce-MOF can be categorized as chemical bonding given its average adsorption energy E of 35.1 kJ/mol and Gibbs free energy $\Delta G°$.[63] In the case of BR46 dye adsorption, it is typical for the NH_2−Ce-MOF to demonstrate a natural and heat-absorbing reaction, as indicated in Table S8.

3.7. Interaction Mechanism. Theories on the mechanisms of BR46 dye adsorption onto NH_2−Ce-MOF may be developed in light of the results of the adsorption investigations in Figure 7(a). As per the text, BR46 dye adsorption in slightly basic conditions is driven by electrostatic attraction. This suggests that the main mechanism driving this process is the electrostatic attraction.[38] The composite material primarily involves the adsorption of N^+ ions due to the electrostatic interaction. The protonated COO^- groups of the glutamic acid component play an important role in facilitating the adsorption of N^+ ions over electrostatic attraction.[64] The primary shape of the BR46 dye molecules is determined in large part by the pH of the solution. By serving as locations for the binding of positively charged N^+ ions, the COO^- groups enhance the overall electrostatic interaction between the adsorbent and the adsorbate. In weakly basic conditions with a pH of 8.0, the BR46 dye primarily consists of positively charged N^+ ions that interact in a favorable manner with the negatively charged places on the NH_2−Ce-MOF. Maximizing the effectiveness and efficiency of adsorbent materials requires an understanding of how electrostatic attraction functions in the adsorption process.[65] Figure 7(b) presents the FTIR spectra for both NH_2−Ce-MOF and BR46@NH_2−Ce-MOF, revealing significant changes in the vibrational patterns of functional groups upon the adsorption of the BR46 dye. This observation implies that an effective interaction has occurred. Specifically, the hydroxyl (−OH) stretching band within the 3200−3500 cm^{-1} range exhibits a decrease in intensity, which suggests the formation of hydrogen bonding between BR46 dye and NH_2−Ce-MOF. Additionally, the peaks associated with C−H stretching, located between 2800−3000 cm^{-1}, show minor shifts and fluctuations in intensity, which can be attributed to interactions with the aromatic components of BR46 dye.[66] The carbonyl (C═O) stretching vibrational peak, typically observed in the range of 1700−1750 cm^{-1}, exhibits a notable shift along with a decline in intensity, which emphasizes its significance in the adsorption process of BR46 dye. Similarly, the C═C aromatic stretching vibrations within the 1500−1600 cm^{-1} range demonstrate marked alterations, indicative of π−π interactions with BR46 dye. Furthermore, shifts and reductions in intensity are evident in bands related to C−N stretching and -NH deformation (1200−1400 cm^{-1}), as well as C−O−C ether groups (1000−1250 cm^{-1}), suggesting underlying chemical interactions at play. The fingerprint region (600−900 cm^{-1}) also indicates additional structural changes resulting from the interaction with BR46 dye. The π−π interaction is also involved in the adsorption of BR46 dye.[67] Hydrogen bonding plays a role in the NH_2−Ce-MOF's capacity to adsorb BR46 dye by forming hydrogen bonds among the oxygen besides nitrogen atoms in the BR46 dye molecules and the hydroxyl groups (−OH) of NH_2−Ce-MOF, influencing its adsorption abilities.[68] Pore filling occurs after the process of adsorption, resulting in a reduction of pore volume besides surface area.

https://doi.org/10.1021/acsomega.4c10666
ACS Omega 2025, 10, 15096−15115

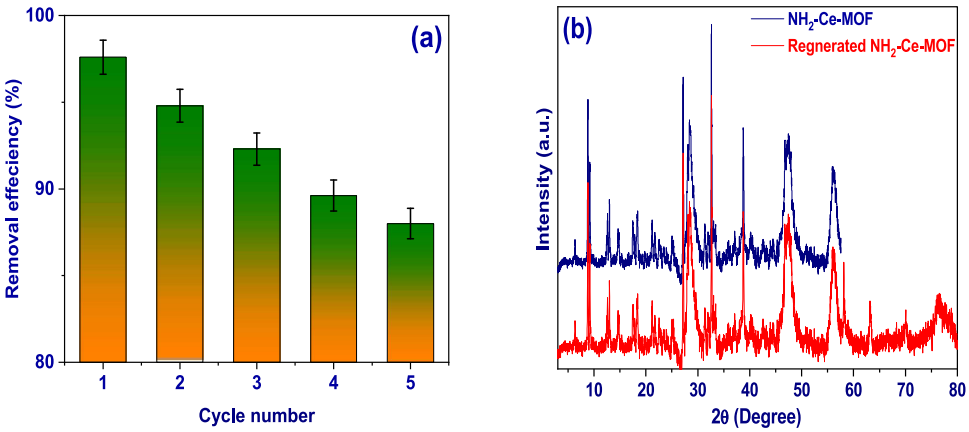

Figure 8. (a) Regeneration efficiency of NH_2−Ce-MOF, and (b) XRD pattern of NH_2−Ce-MOF and regenerated.

3.8. Reusability. The adsorbent was retrieved, and its recyclable nature was inspected in an effort to lower the cost, making, and sustainable use of natural conservation possessions. The BR46 dye solution (25 mL, 300 mg/L) and the adsorbent dose of NH_2−Ce-MOF (0.02 g) were added to a conical flask, which underwent shaking for the repeatability testing. Next adsorption equilibrium, the quantity of remaining BR46 dye was measured. The BR46 dye molecules were extracted from the adsorbent surface using 0.1 mol/L of HCl following the process of washing and rinsing of the filtered NH_2−Ce-MOF with ethanol. After that, the pH was carried to 7. After neutralization with pure water, the finished adsorbent was freeze-dried for further use. The outcomes of the trials that were repeated are shown in Figure 8(a). After five testing cycles, the composite's adsorption efficacy may still be higher than 88%.[69] This suggests that in addition to having a considerable amount of reuse capacity, the adsorbent has an outstanding BR46 dye molecule adsorption capacity. This suggests that in addition to having a significant reusability efficiency, the adsorbent has a good BR46 dye molecule adsorption ability. Following five screening cycles, XRD was used to prove the structure and crystallinity of the adsorbent substantially. Though it was created to be intact, XRD displayed that the element percentages remained constant, representing the adsorbent's resilience during the adsorption procedure. This study validates the high rate of recovery for NH_2−Ce-MOF (Figure 8(b)).[50]

3.9. Comparison with Other Adsorbents. The contrast of the maximal monolayer sorption capabilities (mg/g) of several adsorbents for the adsorption of BR46 dye is displayed in Table S9. It is clear that the adsorbents utilized in this investigation have a higher maximum ability to absorb than the others do.

3.10. Experimental Design Modeling and Response Surface Analysis. *3.10.1. Statistical Analysis.* Statistical modeling is an essential part of researching the effects of independent factors, including pH, contact time, NH_2−Ce-MOF dose, and their interactions. Using data collected from experiments from the modulation RSM-BBD approach, a second-order mathematical polynomial quadratic model has been developed in this respect.[39] An illustration of the polynomial regression model for the colorant BR46 dye adsorption procedure on NH_2−Ce-MOF is provided here. The coded equation is eq 5

$$q_e = 312.908 - 56.4476 \times A + 144.982 \times B - 4.4554 \times C - 38.385 \times AB + 10.3033 \times AC + 17.5571 \times BC + 19.7181 \times A^2 - 129.274 \times B^2 - 32.4919 \times C^2 \quad (5)$$

The equation, which is written in terms of coded factors, can be used to predict the amounts of each reactant. By default, the components' high and low levels are denoted by the numbers +1 and −1, respectively. The impact of each ingredient can be ascertained using the coded equation by comparing the factor coefficients.[28] While the actual equation was eq 6

$$q_e = 18.4223 + -296.538 \times A + 9.42629 \times B + 11.191 \times C + -3.36711 \times AB + 8.58604 \times AC + 0.0739244 \times BC + 342.328 \times A^2 - 0.0572958 \times B^2 - 1.29967 \times C^2 \quad (6)$$

Concentrations of each element and the reaction can be predicted using the equation provided in terms of actual factors. In this case, each aspect's levels should be stated in their original units. Because the coefficients are scaled to suit the units of each element and the intercept is not at the center of the design space, this equation should not be used to calculate the relative influence of each variable.[29] Additionally, the relationship between the actual and projected values for the colorant BR46 dye adsorption capability is displayed in Figure 9(a,b). This graphic makes it evident that the data are distributed to the right, proving without a reasonable question that the experimental findings and statistical projections are properly correlated. Therefore, a good assessment and analysis of the colorant BR46 adsorption on the absorbent surface NH_2−Ce-MOF are provided by the created model.[25]

The Box−Cox plot identifies the optimal power transformation for data, aiming to improve normality, homoscedasticity, or linearity. Here, the *X*-axis represents the power parameter (λ), where values near zero indicate a logarithmic transformation, and the *Y*-axis (Ln(Residual SS)) shows the log of residual sums of squares, with lower values suggesting a better fit. The minimum point on the plot, marked by a green vertical line, likely indicates the optimal (λ), close to zero, with red and blue lines around it, suggesting a confidence interval for effective transformations. For adsorption data of BR46 dye onto NH_2−Ce-MOF, applying this optimal (λ) transformation could improve data distribution symmetry and stabilize

https://doi.org/10.1021/acsomega.4c10666
ACS Omega 2025, 10, 15096−15115

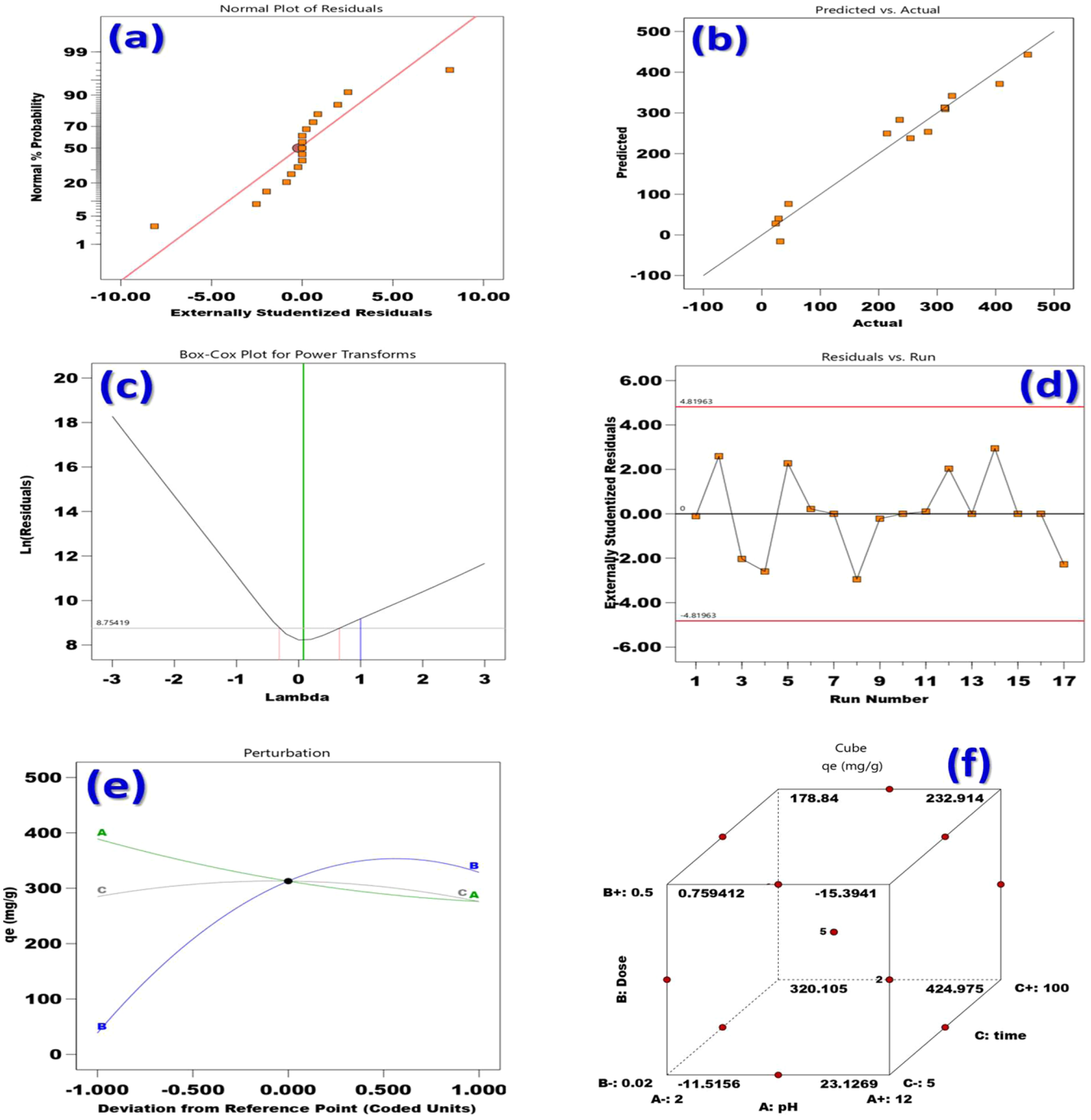

Figure 9. (a) Plots of normal probability for residuals; (b) plots showing the correlation between the investigational and expected values; (c) Box–Cox demonstrates the residuals' modification against lambda; (d) runs with highly standardized residuals vs. residual; (e) plot for perturbation in the rate of response (for A: pH, B: dose, and C: time), and (f) adsorption capability optimization over graphics.

variance, aiding accurate model fitting Figure 9(c). The image shows residuals vs. run plot, which is useful for checking the randomness of residuals across different runs, indicating whether there might be any patterns or issues in the data or model. Here, the *X*-axis characterizes the run number, and the *Y*-axis demonstrates the externally studentized residuals, which measure the difference between observed and predicted values, standardized to account for variability.[70] The plot includes horizontal red lines at ±4.81963, indicating the threshold for identifying outliers; any points outside these lines are potential outliers. The data points appear to fluctuate randomly around zero without any clear pattern, suggesting that the model likely fits the data well and that assumptions of independence and homoscedasticity are likely met. In the context of BR46 dye adsorption on NH_2−Ce-MOF, this randomness in residuals indicates a well-fitting model with no systematic error across different runs (Figure 9(d)).

The perturbation plot illustrates the impact of three variables ((A, B, and C)) on the adsorption capacity (q_e) (mg/g) for BR46 dye onto NH_2−Ce-MOF, with the *X*-axis on behalf of nonconformity from a reference point in coded components and the *Y*-axis presentation (q_e). Each line corresponds to a

https://doi.org/10.1021/acsomega.4c10666
ACS Omega 2025, 10, 15096−15115

Table 1. Analyzing the Fitted Models' Variance

source	sum of Squares	d_f	mean square	F-value	p-value	
model	2.787×10^{05}	9	30970.21	22.24	0.0002	significant
A-dose	25490.67	1	25490.67	18.31	0.0037	
B-time	1.682×10^{05}	1	1.682×10^{05}	120.77	<0.0001	
C-pH	158.80	1	158.80	0.1140	0.7455	
AB	5893.63	1	5893.63	4.23	0.0787	
AC	424.63	1	424.63	0.3050	0.5980	
BC	1233.00	1	1233.00	0.8855	0.3780	
A^2	1637.07	1	1637.07	1.18	0.3142	
B^2	70364.90	1	70364.90	50.53	0.0002	
C^2	4445.14	1	4445.14	3.19	0.1171	
residual	9747.09	7	1392.44			
lack of fit	9747.09	3	3249.03			
pure error	0.0000	4	0.0000			

Table 2. Sum of Squares for Sequential Models

source	sum of squares	d_f	mean square	p-value	adjusted R^2	predicted R^2	
linear	94,670.74	9	10,518.97	0.0018	0.5961	0.3877	
2FI	87,119.48	6	14,519.91	0.8325	0.5168	−0.2411	
quadratic	9747.09	3	3249.03	0.0010	0.9228	0.4594	suggested
cubic	0.0000	0			1.0000		aliased
pure error	0.0000	4	0.0000				

variable: Variable A green line (adsorbent dose) shows a negative trend, indicating that increasing its value reduces (q_e); Variable B blue line (contact time) displays a positive trend, suggesting that higher values enhance (q_e); and Variable C gray line (effect of pH) remains relatively flat, implying a minimal effect on (q_e) within this range. This plot highlights Variable B as having a favorable impact on adsorption capacity, while Variable A has an adverse effect, aiding in identifying which adjustments optimize adsorption efficiency for the BR46 dye onto NH_2−Ce-MOF (Figure 9(e)).

The image shows a three-dimensional (3D) cube plot illustrating the effects of three variables, pH (A), dose (B), and time (C) on the adsorption capability (q_e) of BR46 dye onto NH_2−Ce-MOF. Each corner of the cube represents a unique combination of these variables, with corresponding (q_e) values (mg/g) labeled at each point. This cube plot helps visualize how different levels of each variable impact adsorption capacity, highlighting ideal parameter combinations for maximizing BR46 dye adsorption on NH_2−Ce-MOF (Figure 9(f)).[41]

3.10.2. ANOVA. Using the ANOVA data in Table 1 as evidence, a small value of p (>0.0001) was utilized to show that the model was appropriate for explaining the adsorption process of the colorant BR46. While the high accuracy values below 5% were disregarded due to their insignificance, the strong coefficient of determination R^2 = 0.966 and adjusted-difference R^2 = 0.923 are less than 0.2, demonstrating the development as well, showing that the proposed model had been successfully associated with the actual data.[71] The model is important, as indicated by its low probability value and model F-value of 22.24. The likelihood that an F-value this significant may be caused by noise is less than 0.0001. Model parameters are considered significant when the p-value is less than 0.05. In this instance, the BR46 removal process is greatly impacted by the important model parameters A, C, AB, A^2, and C^2. On the other hand, values above 0.1000, which apply to AC and BC, show that the model parameters are not important. The RSM model correlates with the actual outcomes. Furthermore, it appears that the terms have significantly affected the adsorption capabilities because all of the model's terms had p values less than 0.05. The importance of the selected variables in the adsorption procedure is revealed by the sum of the values in the square. Table 2 represents that the most fitted model was quadratic, and the higher R^2 was 0.922. Table 3 represents that the adsorption capacity experimental was similar to the predicted.

3.10.3. Model Adequacy Checking. It was important to notice that the adsorption capability of NH_2−Ce-MOF for the elimination of BR46 dye decreases with a rise in the adsorbent dose. As the adsorption capability was inversely proportional to

Table 3. Adsorption Capability Data from BR46 and the Response Surface of the Central Composite Structure

	actual variables			yield (mmol/g)		
run	dose (g)	time (min.)	pH	experimental	predicted	residue
1	0.26	52.5	7	312.91	312.91	0.0000
2	0.26	100	2	235.75	283.02	−47.27
3	0.26	5	2	23.61	28.17	−4.57
4	0.26	52.5	7	312.91	312.91	0.0000
5	0.5	52.5	2	254.24	237.84	16.40
6	0.02	52.5	12	325.42	341.82	−16.40
7	0.5	52.5	12	214.09	249.53	−35.44
8	0.26	52.5	7	312.91	312.91	0.0000
9	0.26	5	12	31.42	−15.85	47.27
10	0.26	52.5	7	312.91	312.91	0.0000
11	0.02	52.5	2	406.78	371.34	35.44
12	0.5	5	7	28.48	40.31	−11.83
13	0.02	5	7	45.56	76.43	−30.87
14	0.02	100	7	455.00	443.17	11.83
15	0.26	52.5	7	312.91	312.91	0.0000
16	0.5	100	7	284.38	253.50	30.87
17	0.26	100	12	313.79	309.23	4.57

https://doi.org/10.1021/acsomega.4c10666
ACS Omega 2025, 10, 15096−15115

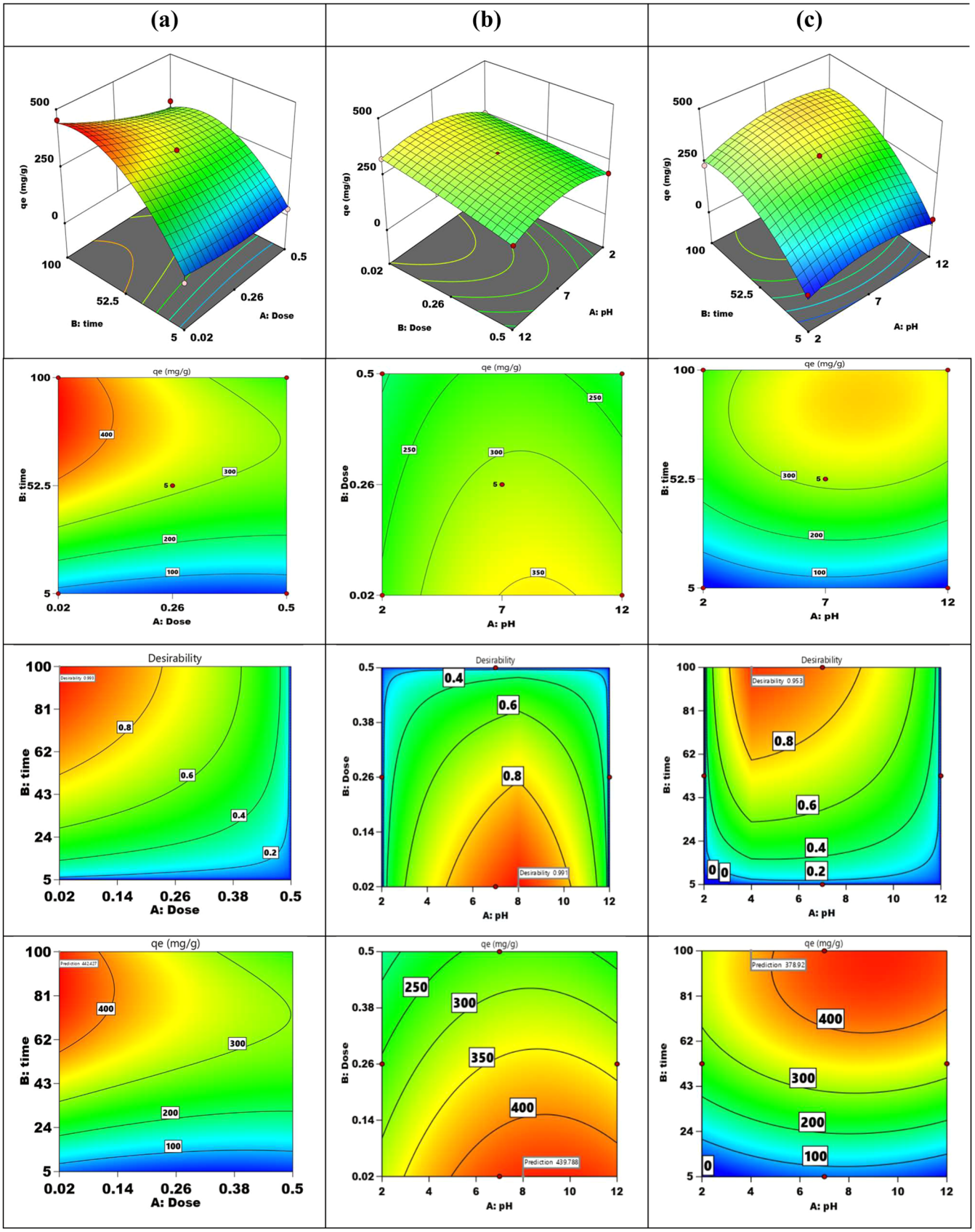

Figure 10. RSM-CCD-derived mutual interaction and desirability analysis of BR46 dye's adsorption capability over NH_2−Ce-MOF: mutual communication of adsorbent dose and pH (A); adsorbent dose (B); and pH and time and time (C).

the adsorbent weight. The simultaneous effects of pH, contact time, and adsorbent dosage between the adsorbent and adsorbate demonstrate a synergistic consequence on adsorption capability. The BR46 adsorption is adversely affected by

https://doi.org/10.1021/acsomega.4c10666
ACS Omega 2025, 10, 15096−15115

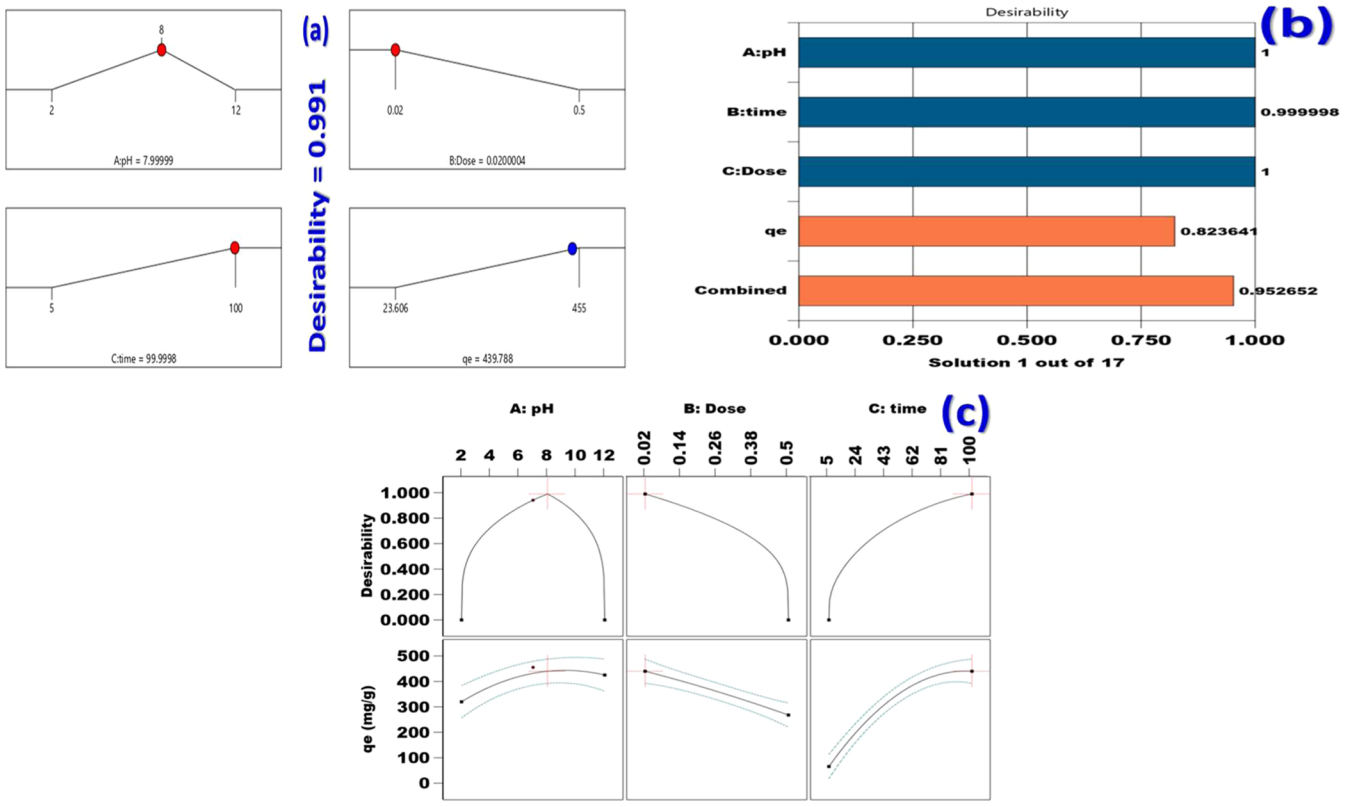

Figure 11. Interest in numerically optimum solutions has increased, (a) desirability of every answer, (b) depiction of separate desirability via a bar graph, and (c) desirability contour of total response interaction.

the quadratically acting parameters that were selected, as well as by the mutually interacting effects of the pH and concentration of the BR46 dye colorant. 3D response surfaces traced according to two input parameters have frequently been employed to comprehend the impacts of interactions among independent elements and to select the optimal adsorption settings for achieving the maximum elimination achievements.[32,33]

Figure 10 displays the 3D reaction curves of the created model based on the mutual interactions of the BR46 dye adsorption process variables. Figure 10(a) makes it obvious that BR46's adsorption capability rises as interaction time and adsorbent dose decrease. At 100 min of contact time and 0.02 g of adsorbent dosage, the maximum adsorption capability was achieved. Figure 10(b) makes it evident that the adsorption capacity of the BR46 dye increases when the adsorbent dose decreases. It increased from 2 to 8 and then decreased from 8 to 12. At pH 8 and an adsorbent dosage of 0.02 g, the maximum adsorption capability was observed. Lastly, Figure 10(c) shows that the maximum adsorption capability occurred at pH 8 and a contact period of 100 min.[72]

3.10.4. Validating Models and Using the Desirability Approach. The desirability function, whose desirability range is 0−1, is used as an optimization tool. A response with a value of 1 is deemed preferred, but a response with a value of 0 is considered far from the approved one. The perfect predicted standards of the investigational variables to obtain the best response (adsorption capability) are exhibited in Figure 11(a). Figure 11(b) shows the outcomes of the desirability functions. Within the specified limits, the maximum response for each experimental factor is provided (i.e., pH = 8, dose of adsorbent 0.02 g, and interaction time = 5−100 min). The experimentation's findings largely agree with the predicted responses.[16] This demonstrated that the model was sufficient and suitable (Figure 11(c)). Two compliance experiments were then conducted using the optimized input variables. This test confirmed the accuracy and efficiency of the BBD in recognizing the ideal adsorption setting for maximum production when joined with the desired function. Consequently, these optimal conditions were used for the subsequent isotherm, kinetic, and thermodynamic studies.[20,21]

4. CONCLUSIONS

The capacity to concurrently extract cationic Basic Red 46 (BR46) dye from an aqueous solution was inspected in this study. Ce-MOF was easily made and thoroughly characterized using a number of techniques after being functionalized with glutamic acid, which contains an amino group, to generate NH_2−Ce-MOF. N_2 adsorption/desorption approved that the synthesized adsorbent has a high surface area of 1158.8 m^2/g, a pore size of 1.511 nm, and a pore volume of 0.875 cm^3/g. Upon the adsorption of the BR46 dye, the surface area decreases to 872.6 m^2/g, the pore size reduces to 1.18 nm, and the pore volume drops to 0.53 cm^3/g. Since the dye particles can effectively occupy the micropores, the decreases in the surface area, pore size, and volume demonstrates the material's effective adsorption capability. 454.8 mg/g greater adsorption capabilities were demonstrated. The pseudo-second-order kinetic model besides the Langmuir isotherm model, respectively, were the most effective in simulating adsorption kinetics, and isotherm curves, displaying an adsorption energy of 28.4 kJ/mol and chemisorption van der Waals force, $\pi-\pi$ conjugation, electrostatic contact, hydrogen bonding, and pore filling were the main adsorption driving forces. The findings

https://doi.org/10.1021/acsomega.4c10666
ACS Omega 2025, 10, 15096−15115

may offer theoretical and technical support for the elimination of cationic dyes via simultaneous adsorption. Through the study of the effect of temperature, it was confirmed that the adsorption technique was endothermic as the positive charge of ΔH°. The spontaneous increase in the negativity of ΔG° upon increasing the temperature and the increase in the randomness with rising temperature as ΔS° was 289.32 J/mol K. Enhanced results of the adsorption process through the utilization of the Box−Behnken design (BBD) and Response Surface Methodology (RSM). Given that the adsorbent was made of reusable materials and could be reused more than five times with high efficiency, the NH_2−Ce-MOF offers a viable low-cost option for removing BR46 dye from wastewater streams.

■ ASSOCIATED CONTENT

Data Availability Statement

All data generated or analyzed during this study are included in the article (and the Supporting Information).

Supporting Information

The Supporting Information is available free of charge at https://pubs.acs.org/doi/10.1021/acsomega.4c10666.

Chemical name, formula, and company (Table S1), instruments and equipments (Table S2), true variables, codes, and their BBD levels (Table S3), crystallographic data (Table S4), equations used in this work to fit the data of adsorption experiments (Table S5), parameter of the adsorption isotherm for BR46 on NH_2−Ce-MOF (Table S6), models of adsorption kinetic parameters of BR46 on NH_2−Ce-MOF (Table S7), thermodynamic parameters (Table S8), and different adsorbents' BR46 adsorption capacities (Table S9) (PDF)

■ AUTHOR INFORMATION

Corresponding Author

Nashwa M. El-Metwaly − *Department of Chemistry, Faculty of Sciences, Umm Al-Qura University, Makkah 24382, Saudi Arabia; Department of Chemistry, Faculty of Science, Mansoura University, Mansoura 35516, Egypt;* orcid.org/0000-0002-0619-6206; Email: n_elmetwaly00@yahoo.com, nmmohamed@uqu.edu.sa

Authors

Roaa T. Mogharbel − *Department of Chemistry, College of Science, Northern Border University, Arar 91431, Saudi Arabia*

Omaymah Alaysuy − *Department of Chemistry, College of Science, University of Tabuk, Tabuk 47512, Saudi Arabia*

Ibrahim Saleem S Alatawi − *Department of Chemistry, College of Science, University of Tabuk, Tabuk 47512, Saudi Arabia*

Nadiyah M. Alshammari − *Department of Chemistry, College of Science, Qassim University, 51452 Buraidah, Saudi Arabia*

Sahar Sallam − *Department of Physical Science, Physics/Chemistry Division, Jazan University, 45142 Jazan, Saudi Arabia*

Abeer M. Almutairi − *Department of Physics, Faculty of Science, University of Tabuk, Tabuk 71421, Saudi Arabia*

Ameena Mohsen Al-Bonayan − *Department of Chemistry, Faculty of Sciences, Umm Al-Qura University, Makkah 24382, Saudi Arabia*

Complete contact information is available at: https://pubs.acs.org/10.1021/acsomega.4c10666

Notes

The authors declare no competing financial interest.

■ ACKNOWLEDGMENTS

The authors extend their appreciation to the Deanship of Scientific Research at Northern Border University, Arar, KSA for funding this research work through the project number "NBU-FFR-2025-2414-03".

■ REFERENCES

(1) Benhalima, T.; Sadi, A.; Dairi, N.; Ferfera-Harrar, H. Multifunctional carboxymethyl cellulose-dextran sulfate/AgNPs@zeolite hydrogel beads for basic red 46 and methylene blue dyes removal and water disinfection control. *Sep. Purif. Technol.* **2024**, *342*, No. 127001.

(2) Karaca, C.; Karaca, M.; Kıranşan, M.; Karaca, S.; Açışlı, Ö.; Gürses, A. Comparison of the removal efficiencies of Basic red 46 from aqueous solutions using Aşkale lignite with and without ultrasound assisted processes. *Desalin. Water Treat.* **2023**, *315*, 111−121.

(3) Jadhav, S.; Jaspal, D. Elimination of cationic azodye from aqueous media using doped polyaniline (PANI): Adsorption optimization and modeling. *Can. J. Chem.* **2020**, *98*, 717−724.

(4) Behpour, M.; Ramezani, Z.; Masoum, S. Simultaneous removal of Basic Blue41 and Basic Red46 dyes in binary aqueous systems via activated carbon from palm bio-waste: optimization by central composite design, equilibrium, kinetic, and thermodynamic studies. *Environ. Technol. Innovation* **2021**, *24*, No. 102039.

(5) Rahimi, K.; Mirzaei, R.; Akbari, A.; Mirghaffari, N. Preparation of nanoparticle-modified polymeric adsorbent using wastage fuzzes of mechanized carpet and its application in dye removal from aqueous solution. *J. Cleaner Prod.* **2018**, *178*, 373−383.

(6) Paredes-Quevedo, L. C.; Castellanos, N. J.; Carriazo, J. G. Influence of porosity and surface area of a modified kaolinite on the adsorption of basic red 46 (BR-46). *Water, Air, Soil Pollut.* **2021**, *232*, No. 509.

(7) Karim, A. B.; Mounir, B.; Hachkar, M.; Bakasse, M.; Yaacoubi, A. Removal of Basic Red 46 dye from aqueous solution by adsorption onto Moroccan clay. *J. Hazard. Mater.* **2009**, *168*, 304−309.

(8) Moradi, O. Adsorption behavior of basic red 46 by single-walled carbon nanotubes surfaces. *Fullerenes, Nanotubes Carbon Nanostruct.* **2013**, *21*, 286−301.

(9) El-Aziz, M. A.; Youssef, A. M.; Kamal, K. H.; Kelnar, I.; Kamel, S. Preparation and performance of bionanocomposites based on grafted chitosan, GO and TiO2-NPs for removal of lead ions and basic-red 46. *Carbohydr. Polym.* **2023**, *305*, No. 120571.

(10) Benhalima, T.; Chicha, W.; Ferfera-Harrar, H. Sponge-like biodegradable polypyrrole-modified biopolymers for selective adsorption of basic red 46 and crystal violet dyes from single and binary component systems. *Int. J. Biol. Macromol.* **2023**, *253*, No. 127532.

(11) Bouatay, F.; Dridi-Dhaouadi, S.; Drira, N. M. Farouk Mhenni, Application of modified clays as an adsorbent for the removal of Basic Red 46 and Reactive Yellow 181 from aqueous solution. *Desalin. Water Treat.* **2016**, *57*, 13561−13572.

(12) Nassef, H. M.; Al-Hazmi, G. A. A. M.; Alayyafi, A. A.; El-Desouky, M. G.; El-Bindary, A. A. Synthesis and characterization of new composite sponge combining of metal-organic framework and chitosan for the elimination of Pb(II), Cu(II) and Cd(II) ions from aqueous solutions: Batch adsorption and optimization using Box-Behnken design. *J. Mol. Liq.* **2024**, *394*, No. 123741, DOI: 10.1016/j.molliq.2023.123741.

(13) El-Wahab, M. A.; El-Desouky, M. G. In silico antibacterial, anticancer, antioxidant, antidiabetic activity predictions of the dual organic peroxide 2,5-dimethyl-2,5-di(tert-butyl peroxyl)hexane. *Main Group Chem.* **2024**, *23*, 177−190.

(14) Alsuhaibani, A. M.; Alayyafi, A. A.; Albedair, L. A.; El-Desouky, M. G.; El-Bindary, A. A. Synthesis and characterization of metal−organic frameworks based on thorium for the effective removal of 2,4-dichlorophenylacetic pesticide from water: Batch adsorption and Box-Behnken Design optimization, and evaluation of reusability. *J. Mol. Liq.* **2024**, *398*, No. 124252, DOI: 10.1016/j.molliq.2024.124252.
(15) Mogharbel, R. T.; Alkhamis, K.; Felaly, R.; El-Desouky, M. G.; El-Bindary, A. A.; El-Metwaly, N. M.; El-Bindary, M. A. Superior adsorption and removal of industrial dye from aqueous solution via magnetic silver metal-organic framework nanocomposite. *Environ. Technol.* **2024**, *45*, 2558−2574.
(16) El-Fattah, W. A.; Guesmi, A.; Hamadi, N. B.; Houas, A.; Alotaibi, M. T.; El-Desouky, M. G.; Shahat, A. Novel composite from chitosan and a metal-organic framework for removal of tartrazine dye from aqueous solutions; adsorption isotherm, kinetic, and optimization using Box-Benkhen design. *Int. J. Biol. Macromol.* **2024**, *273*, No. 133015, DOI: 10.1016/j.ijbiomac.2024.133015.
(17) El-Fattah, W. A.; Guesmi, A.; Ben Hamadi, N.; El-Desouky, M. G.; Shahat, A. A green synthesis of cellulose nanocrystals biosorbent for remediation of wastewater containing industrial dye. *Colloids Surf., A* **2024**, *681*, No. 132729, DOI: 10.1016/j.colsurfa.2023.132729.
(18) AlSalem, H. S.; Alatawi, R. A. S.; Bukhari, A. A. H.; Alnawmasi, J. S.; Zghab, I.; El-Desouky, M. G.; Almabadi, M. H.; Alnakhli, Z. H.; Elsayed, N. H. Adsorption and removal of Pb (II) via layer double hydroxide encapsulated with chitosan; synthesis, characterization adsorption isotherms, kinetics, thermodynamics, & optimization via Box-Behnken design. *Int. J. Biol. Macromol.* **2024**, *283*, No. 137517, DOI: 10.1016/j.ijbiomac.2024.137517.
(19) Siddiq, H. A.; Madkhali, M. M. M.; Ghubayra, R.; Alaghaz, A. N. M. A.; El-Desouky, M. G.; El-Bindary, M. A.; El-Bindary, A. A. Efficient removal of tetracycline by VCo-layered double hydroxide encapsulated with chitosan: Optimization via Box-Behnken design, and thermodynamics. *Int. J. Biol. Macromol.* **2025**, *296*, No. 139565, DOI: 10.1016/j.ijbiomac.2025.139565.
(20) El-Desouky, M. G.; Alayyafi, A. A.; Al-Hazmi, G. A. A. M.; El-Bindary, A. A. Effect of metal organic framework alginate aerogel composite sponge on adsorption of tartrazine from aqueous solutions: Adsorption models, thermodynamics and optimization via Box-Behnken design. *J. Mol. Liq.* **2024**, *399*, No. 124392, DOI: 10.1016/j.molliq.2024.124392.
(21) Alsuhaibani, A. M.; Alayyafi, A. A.; Albedair, L. A.; El-Desouky, M. G.; El-Bindary, A. A. Efficient fabrication of a composite sponge for Cr(VI) removal via citric acid cross-linking of metal-organic framework and chitosan: Adsorption isotherm, kinetic studies, and optimization using Box-Behnken design. *Mater. Today Sustainability* **2024**, *26*, No. 100732, DOI: 10.1016/j.mtsust.2024.100732.
(22) Almahri, A.; Morad, M.; Aljohani, M. M.; Alatawi, N. M.; Saad, F. A.; Abumelha, H. M.; El-Desouky, M. G.; El-Bindary, A. A. Atrazine reclamation from an aqueous environment using a ruthenium-based metal-organic framework. *Process Saf. Environ. Prot.* **2023**, *177*, 52−68.
(23) Yue, J.; Li, Z.; Liu, X.; Wu, Z.; Wang, J.; Tu, M.; Shi, H.; Fan, D.; Li, Y. Glu@ Zn-Ni MOF Constructed Through Ligand Exchange for Bi-Enzyme Immobilization With Improved Performance in Rare Ginsenoside Production. *Appl. Organomet. Chem.* **2024**, No. e7867.
(24) Almahri, A.; Abou-Melha, K. S.; Katouah, H. A.; Al-bonayan, A. M.; Saad, F. A.; El-Desouky, M. G.; El-Bindary, A. A. Adsorption and removal of the harmful pesticide 2,4-dichlorophenylacetic acid from an aqueous environment via coffee waste biochar: Synthesis, characterization, adsorption study and optimization via Box-Behnken design. *J. Mol. Struct.* **2023**, *1293*, No. 136238, DOI: 10.1016/j.molstruc.2023.136238.
(25) Al-Hazmi, G. A. A. M.; Alayyafi, A. A.; El-Desouky, M. G.; El-Bindary, A. A. Chitosan-nano CuO composite for removal of mercury (II): Box-Behnken design optimization and adsorption mechanism. *Int. J. Biol. Macromol.* **2024**, *261*, No. 129769, DOI: 10.1016/j.ijbiomac.2024.129769.
(26) Alluhaybi, A. A.; Alharbi, A.; Alshammari, K. F.; El-Desouky, M. G. Efficient Adsorption and Removal of the Herbicide 2,4-Dichlorophenylacetic Acid from Aqueous Solutions Using MIL-88(Fe)-NH2. *ACS Omega* **2023**, *8*, 40775−40784.
(27) Al-Qahtani, S. D.; Alhasani, M.; Alkhathami, N.; Al-Ola, K. A. A.; Alkhamis, K.; El-Desouky, M. G.; El-Bindary, A. A. Effective levofloxacin adsorption and removal from aqueous solution onto tea waste biochar; synthesis, characterization, adsorption studies, and optimization by Box−Behnken design and its antibacterial activity. *Environ. Technol.* **2024**, *45*, 4928−4950.
(28) Alotaibi, A. M.; Alnawmasi, J. S.; Alshammari, N. A. H.; Abomuti, M. A.; Elsayed, N. H.; El-Desouky, M. G. Industrial dye absorption and elimination from aqueous solutions through bio-composite construction of an organic framework encased in food-grade algae and alginate: Adsorption isotherm, kinetics, thermodynamics, and optimization by Box−Behnken design. *Int. J. Biol. Macromol.* **2024**, *274*, No. 133442, DOI: 10.1016/j.ijbiomac.2024.133442.
(29) Al-Hazmi, G. H.; Albedair, L. A.; Alatawi, R. A. S.; Alnawmasi, J. S.; Alsuhaibani, A. M.; El-Desouky, M. G. Enhancing trimethoprim pollutant removal from wastewater using magnetic metal-organic framework encapsulated with poly (itaconic acid)-grafted crosslinked chitosan composite sponge: Optimization through Box-Behnken design and thermodynamics of adsorption parameters. *Int. J. Biol. Macromol.* **2024**, *268*, No. 131947, DOI: 10.1016/j.ijbiomac.2024.131947.
(30) Aljohani, M. M.; Al-Qahtani, S. D.; Alshareef, M.; El-Desouky, M. G.; El-Bindary, A. A.; El-Metwaly, N. M.; El-Bindary, M. A. Highly efficient adsorption and removal bio-staining dye from industrial wastewater onto mesoporous Ag-MOFs. *Process Saf. Environ. Prot.* **2023**, *172*, 395−407.
(31) Alsharief, H. H.; Alatawi, N. M.; Al-bonayan, A. M.; Alrefaee, S. H.; Saad, F. A.; El-Desouky, M. G.; El-Bindary, A. A. Adsorption of Azorubine E122 dye via Na-mordenite with tryptophan composite: batch adsorption, Box−Behnken design optimization and antibacterial activity. *Environ. Technol.* **2023**, *45*, 3496−3515, DOI: 10.1080/09593330.2023.2219399.
(32) Alrefaee, S. H.; Aljohani, M.; Alkhamis, K.; Shaaban, F.; El-Desouky, M. G.; El-Bindary, A. A.; El-Bindary, M. A. Adsorption and effective removal of organophosphorus pesticides from aqueous solution via novel metal-organic framework: Adsorption isotherms, kinetics, and optimization via Box-Behnken design. *J. Mol. Liq.* **2023**, *384*, No. 122206, DOI: 10.1016/j.molliq.2023.122206.
(33) Alsuhaibani, A. M.; Refat, M. S.; Adam, A. M. A.; El-Desouky, M. G.; El-Bindary, A. A. Enhanced adsorption of ceftriaxone antibiotics from water by mesoporous copper oxide nanosphere. *Desalin. Water Treat.* **2023**, *281*, 234−248.
(34) Al-Hazmi, G. H.; Adam, A. M. A.; El-Desouky, M. G.; ElBindary, A. A.; Alsuhaibani, A. M.; Refat, M. S. Efficient adsorption of Rhodamine B using a composite of Fe3O4@ zif-8: Synthesis, characterization, modeling analysis, statistical physics and mechanism of interaction. *Bull. Chem. Soc. Ethiop.* **2022**, *37*, 211−229.
(35) El-Metwaly, N. M.; Katouah, H. A.; El-Desouky, M. G.; El-Bindary, A. A.; El-Bindary, M. A. Fabricating of Fe3O4@Ag-MOF nanocomposite and evaluating its adsorption activity for removal of doxorubicin. *J. Environ. Sci. Health, Part A* **2022**, *57*, 1099−1115.
(36) El-Desouky, M. G.; Shahat, A.; El-Bindary, A. A.; El-Bindary, M. A. Description, kinetic and equilibrium studies of the adsorption of carbon dioxide in mesoporous iron oxide nanospheres. *Biointerface Res. Appl. Chem.* **2022**, *12*, 1022−1038.
(37) El-Desouky, M. G.; Khalil, M. A. G.; El-Afify, M. A. M.; El-Bindary, A. A.; El-Bindary, M. A. Effective methods for removing different types of dyes − modelling analysisstatistical physics treatment and DFT calculations: a review. *Desalin. Water Treat.* **2022**, *280*, 89−127.
(38) El-Desouky, M. G.; Khalil, M. A.; El-Bindary, A. A.; El-Bindary, M. A. Biological, biochemical and thermochemical techniques for biofuel production: An updated review. *Biointerface Res. Appl. Chem.* **2022**, *12*, 3034−3054.
(39) Alsharief, H. H.; Alatawi, N. M.; Al-bonayan, A. M.; Alrefaee, S. H.; Saad, F. A.; El-Desouky, M. G.; El-Bindary, A. A. Adsorption of

Azorubine E122 dye via Na-mordenite with tryptophan composite: batch adsorption, Box−Behnken design optimization and antibacterial activity. *Environ. Technol.* **2024**, *45*, 3496−3515.
(40) El-Desouky, M. G.; El-Bindary, A. A. Magnetic metal-organic framework (Fe3O4@ZIF-8) nanocomposites for adsorption of anionic dyes from wastewater. *Inorg. Nano-Met. Chem.* **2024**, *54*, 81−95.
(41) Al-Hazmi, G. A. A.; El-Zahhar, A. A.; El-Desouky, M. G.; El-Bindary, A. Superior adsorption and removal of doxorubicin from aqueous solution using activated carbon via thermally treated green adsorbent: isothermal, kinetic, and thermodynamic studies. *Environ. Technol.* **2024**, *45*, 1969−1988.
(42) El-Desouky, M. G.; El-Bindary, A. A.; El-Bindary, M. A. Low-temperature adsorption study of carbon dioxide on porous magnetite nanospheres iron oxide. *Biointerface Res. Appl. Chem.* **2022**, *12*, 6252−6268.
(43) El-Desouky, M. G.; El-Bindary, A. A.; El-Afify, M. A. M.; Hassan, N. Synthesis, characterization, theoretical calculation, DNA binding, molecular docking, anticovid-19 and anticancer chelation studies of some transition metal complexes. *Inorg. Nano-Met. Chem.* **2022**, *52*, 1273−1288.
(44) El-Desouky, M. G.; Abd El-Wahab, M.; El-Bindary, A. A. Interpretations and DFT calculations for polypropylene/cupper oxide nanosphere. *Biointerface Res. Appl. Chem.* **2022**, *12*, 1134−1147.
(45) El-Bindary, M. A.; El-Desouky, M. G.; El-Bindary, A. A. Metal−organic frameworks encapsulated with an anticancer compound as drug delivery system: Synthesis, characterization, antioxidant, anticancer, antibacterial, and molecular docking investigation. *Appl. Organomet. Chem.* **2022**, *36*, No. e6660, DOI: 10.1002/aoc.6660.
(46) Langmuir, I. The constitution and fundamental properties of solids and liquids. Part I. Solids. *J. Am. Chem. Soc.* **1916**, *38*, 2221−2295.
(47) Freundlich, H. M. F. Over the adsorption in solution. *J. Phys. Chem. A* **1906**, *57*, 385−471.
(48) Tempkin, M. I.; Pyzhev, V. J. Kinetics of ammonia synthesis on promoted iron catalyst. *Acta Phys. Chim. USSR* **1940**, *12*, 327−356.
(49) Alsuhaibani, A. M.; Refat, M. S.; Atta, A. A.; El-Desouky, M. G.; El-Bindary, A. A. Efficient adsorption and removal of tetracycline antibiotics from aqueous solutions onto nickel oxide nanoparticles via organometallic chelate. *Desalin. Water Treat.* **2022**, *277*, 190−205.
(50) Al-Hazmi, G. H.; Refat, M. S.; El-Desouky, M. G.; El-Bindary, A. A. Effective adsorption and removal of industrial dye from aqueous solution using mesoporous zinc oxide nanoparticles via metal organic frame work: equilibrium, kinetics and thermodynamic studies. *Desalin. Water Treat.* **2022**, *272*, 277−289.
(51) El-Bindary, M. A.; El-Desouky, M. G.; El-Bindary, A. A. Adsorption of industrial dye from aqueous solutions onto thermally treated green adsorbent: A complete batch system evaluation. *J. Mol. Liq.* **2022**, *346*, No. 117082, DOI: 10.1016/j.molliq.2021.117082.
(52) Dubinin, M. The equation of the characteristic curve of activated charcoal. *Dokl. Akad. Nauk SSSR* **1947**, *55*, 327−329.
(53) El-Bindary, A. A.; El-Desouky, M. G.; El-Afify, M. A. M. Thermal and spectroscopic studies of some prepared metal complexes and investigation of their potential anticancer and antiviral drug activity against SARS-CoV-2 by molecular docking simulation. *Biointerface Res. Appl. Chem.* **2022**, *12*, 1053−1075.
(54) Al-Wasidi, A. S.; AlZahrani, I. I. S.; Thawibaraka, H. I.; Naglah, A. M.; El-Desouky, M. G.; El-Bindary, M. A. Adsorption studies of carbon dioxide and anionic dye on green adsorbent. *J. Mol. Struct.* **2022**, *1250*, No. 131736, DOI: 10.1016/j.molstruc.2021.131736.
(55) Al-Hazmi, G. H.; Refat, M. S.; El-Desouky, M. G.; Wali, F. K. M.; El-Bindary, A. A. Effective removal of industrial dye from aqueous solution using mesoporous nickel oxide: a complete batch system evaluation. *Desalin. Water Treat.* **2022**, *273*, 246−260.
(56) Altalhi, T. A.; Ibrahim, M. M.; Mersal, G. A. M.; Mahmoud, M. H. H.; Kumeria, T.; El-Desouky, M. G.; El-Bindary, A. A.; El-Bindary, M. A. Adsorption of doxorubicin hydrochloride onto thermally treated green adsorbent: Equilibrium, kinetic and thermodynamic studies. *J. Mol. Struct.* **2022**, *1263*, No. 133160, DOI: 10.1016/j.molstruc.2022.133160.
(57) Lagergren, S. K. About the theory of so-called adsorption of soluble substances. *Sven. Vetenskapsakad. Handingarl* **1898**, *24*, 1−39.
(58) Ho, Y.-S.; McKay, G. Sorption of dye from aqueous solution by peat. *Chem. Eng. J.* **1998**, *70*, 115−124.
(59) Weber, W. J., Jr; Morris, J. C. Kinetics of adsorption on carbon from solution. *J. Sanit. Eng. Div.* **1963**, *89*, 31−59.
(60) Dehghani, M. H.; Dehghan, A.; Najafpoor, A. Removing Reactive Red 120 and 196 using chitosan/zeolite composite from aqueous solutions: Kinetics, isotherms, and process optimization. *J. Ind. Eng. Chem.* **2017**, *51*, 185−195.
(61) Lima, E. C.; Hosseini-Bandegharaei, A.; Moreno-Piraján, J. C.; Anastopoulos, I. A critical review of the estimation of the thermodynamic parameters on adsorption equilibria. Wrong use of equilibrium constant in the Van't Hoof equation for calculation of thermodynamic parameters of adsorption. *J. Mol. Liq.* **2019**, *273*, 425−434.
(62) Tran, H. N.; You, S.-J.; Hosseini-Bandegharaei, A.; Chao, H.-P. Mistakes and inconsistencies regarding adsorption of contaminants from aqueous solutions: a critical review. *Water Res.* **2017**, *120*, 88−116.
(63) Oladipo, B.; Govender-Opitz, E.; Ojumu, T. V. Kinetics, thermodynamics, and mechanism of Cu (II) ion sorption by biogenic iron precipitate: using the lens of wastewater treatment to diagnose a typical biohydrometallurgical problem. *ACS Omega* **2021**, *6*, 27984−27993.
(64) Yang, X.; Zhu, W.; Song, Y.; Zhuang, H.; Tang, H. Removal of cationic dye BR46 by biochar prepared from Chrysanthemum morifolium Ramat straw: A study on adsorption equilibrium, kinetics and isotherm. *J. Mol. Liq.* **2021**, *340*, No. 116617.
(65) Fu, Y.; Xu, Y.; Lou, B.; Qin, X.; Zhang, L.; Yuan, H.; Zhang, L.; Zhang, Y.; Lu, J. Magnetically recyclable core−shell MOF nanoparticles of Fe 3 O 4@ PDA@ UIO-66-NH 2 grafted by organic acids for intensified cationic dye adsorption. *New J. Chem.* **2022**, *46*, 11071−11081.
(66) Al-Hazmi, G. H.; Albedair, L. A.; Alatawi, R. A.; Alsuhaibani, A. M.; Bukhari, A. A. H.; El-Bindary, A. A. Effective synthesis and characterization of citric acid cross-linking of modified ferrous metal-organic framework and chitosan nanocomposite sponge for Th (IV) elimination: Adsorption isotherms, kinetic analysis, and optimization by Box-Behnken design. *Int. J. Biol. Macromol.* **2024**, *281*, No. 136194.
(67) Xiao, C.; Liu, X.; Mao, S.; Zhang, L.; Lu, J. Sub-micron-sized polyethylenimine-modified polystyrene/Fe3O4/chitosan magnetic composites for the efficient and recyclable adsorption of Cu (II) ions. *Appl. Surf. Sci.* **2017**, *394*, 378−385.
(68) Wu, S.; Wang, F.; Yuan, H.; Zhang, L.; Mao, S.; Liu, X.; Alharbi, N. S.; Rohani, S.; Lu, J. Fabrication of xanthate-modified chitosan/poly (N-isopropylacrylamide) composite hydrogel for the selective adsorption of Cu (II), Pb (II) and Ni (II) metal ions. *Chem. Eng. Res. Des.* **2018**, *139*, 197−210.
(69) AlHazmi, G. A. A.; AbouMelha, K. S.; El-Desouky, M. G.; El-Bindary, A. A. Effective adsorption of doxorubicin hydrochloride on zirconium metal-organic framework: Equilibrium, kinetic and thermodynamic studies. *J. Mol. Struct.* **2022**, *1258*, No. 132679, DOI: 10.1016/j.molstruc.2022.132679.
(70) Al-Hazmi, G. A. A. M.; Alayyafi, A. A.; El-Desouky, M. G.; El-Bindary, A. A. Guava seed activated carbon loaded calcium alginate aerogel for the adsorption of diclofenac sodium: Characterization, isotherm, kinetics, and optimization via Box-Behnken design. *Int. J. Biol. Macromol.* **2024**, *262*, No. 129995, DOI: 10.1016/j.ijbiomac.2024.129995.
(71) Al-Hazmi, G. A. A.; El-Zahhar, A. A.; El-Desouky, M. G.; El-Bindary, M. A.; El-Bindary, A. A. Efficiency of Fe3O4@ZIF-8 for the removal of Doxorubicin from aqueous solutions: equilibrium, kinetics and thermodynamic studies. *Environ. Technol.* **2024**, *45*, 731−750.
(72) Al-Qahtani, S. D.; Alhasani, M.; Alkhathami, N.; Al-Ola, K. A. A.; Alkhamis, K.; El-Desouky, M. G.; El-Bindary, A. A. Effective levofloxacin adsorption and removal from aqueous solution onto tea

waste biochar; synthesis, characterization, adsorption studies, and optimization by Box−Behnken design and its antibacterial activity. *Environ. Technol.* **2023**, *45*, 4928−4950, DOI: 10.1080/09593330.2023.2283409.

https://doi.org/10.1021/acsomega.4c10666
ACS Omega 2025, 10, 15096−15115